EMBO
Molecular Medicine

Altered γ-secretase activity in mild cognitive impairment and Alzheimer's disease

Nobuto Kakuda[1,2,3], Mikio Shoji[4], Hiroyuki Arai[5], Katsutoshi Furukawa[5], Takeshi Ikeuchi[6], Kohei Akazawa[7], Mako Takami[2,3], Hiroyuki Hatsuta[8], Shigeo Murayama[8], Yasuhiro Hashimoto[9], Masakazu Miyajima[10], Hajime Arai[10], Yu Nagashima[11], Haruyasu Yamaguchi[12], Ryozo Kuwano[13], Kazuhiro Nagaike[1], Yasuo Ihara[2,14,3], the Japanese Alzheimer's Disease Neuroimaging Initiative*

Keywords: amyloid β-protein; CSF; γ-secretase; NSAID; stepwise processing

DOI 10.1002/emmm.201200214

Received December 21, 2010
Revised December 22, 2011
Accepted January 09, 2012

We investigated why the cerebrospinal fluid (CSF) concentrations of Aβ42 are lower in mild cognitive impairment (MCI) and Alzheimer's disease (AD) patients. Because Aβ38/42 and Aβ40/43 are distinct product/precursor pairs, these four species in the CSF together should faithfully reflect the status of brain γ-secretase activity, and were quantified by specific enzyme-linked immunosorbent assays in the CSF from controls and MCI/AD patients. Decreases in the levels of the precursors, Aβ42 and 43, in MCI/AD CSF tended to accompany increases in the levels of the products, Aβ38 and 40, respectively. The ratios Aβ40/43 *versus* Aβ38/42 in CSF (each representing cleavage efficiency of Aβ43 or Aβ42) were largely proportional to each other but generally higher in MCI/AD patients compared to control subjects. These data suggest that γ-secretase activity in MCI/AD patients is enhanced at the conversion of Aβ43 and 42 to Aβ40 and 38, respectively. Consequently, we measured the *in vitro* activity of raft-associated γ-secretase isolated from control as well as MCI/AD brains and found the same, significant alterations in the γ-secretase activity in MCI/AD brains.

INTRODUCTION

Senile plaques, the neuropathological hallmark of Alzheimer's disease (AD), are composed of amyloid β-protein (Aβ). Aβ is derived from β-amyloid precursor protein (APP) through sequential cleavage by β- and γ-secretases. β-Secretase cleaves at the luminal portion (β-site) of APP to generate a β-carboxyl terminal fragment of APP (βCTF), an immediate substrate of γ-secretase, to produce different Aβ species (for a review see Selkoe, 2001). The most abundant secreted Aβ species is Aβ40,

(1) Immuno-Biological Laboratories Co., Fujioka, Japan
(2) Faculty of Life and Medical Sciences, Department of Neuropathology, Doshisha University, Kyoto, Japan
(3) New Energy and Industrial Technology Development Organization (NEDO), Kanagawa, Japan
(4) Department of Neurology, Institute of Brain Science, Hirosaki University Graduate School of Medicine, Hirosaki, Japan
(5) Division of Brain Sciences, Department of Geriatrics and Gerontology, Institute of Development, Aging and Cancer, Tohoku University, Sendai, Japan
(6) Department of Neurology, Brain Research Institute, Niigata University, Niigata, Japan
(7) Department of Medical Informatics, Niigata University Medical and Dental Hospital, Niigata, Japan
(8) Department of Neuropathology, Tokyo Metropolitan Institute of Gerontology, Tokyo, Japan
(9) Department of Biochemistry, Fukushima Medical University, Fukushima, Japan
(10) Department of Neurosurgery, Juntendo University School of Medicine, Tokyo, Japan
(11) Department of Neurology, Graduate School of Medicine, University of Tokyo, Tokyo, Japan
(12) Gunma University School of Health Sciences, Maebashi, Japan
(13) Department of Molecular Genetics, Bioresource Science Branch, Center for Bioresources, Niigata University, Niigata, Japan
(14) Core Research for Evolutional Science and Technology (CREST), Japan Science and Technology Corporation, Tokyo, Japan
***Corresponding author:** Tel: +81 774 656058; Fax: +81 774 731922;
E-mail: yihara@mail.doshisha.ac.jp

whereas the species that has two extra residues (Aβ42) is a minor one (<10%); however, the latter is the one that deposits first and predominates in senile plaques (Iwatsubo et al, 1994).

Presenilin 1/2 make up the catalytic site of γ-secretase. The enzymatic properties of γ-secretase that cleave the transmembrane domain of βCTF have been an enigma, although recent studies provided partial elucidation of this mechanism (Qi-Takahara et al, 2005; Takami et al, 2009). γ-Secretase has two product lines, which successively convert the Aβ49 and Aβ48 that are generated by ε-cleavage, to shorter Aβs by releasing tri- or tetrapeptides in a stepwise fashion. Aβ49 is successively cleaved mostly into Aβ40 via Aβ46 and Aβ43, while Aβ48 is similarly cleaved into Aβ38 via Aβ45 and Aβ42 (see Fig 1). Importantly, the differences between the amounts of released tri- and tetrapeptides determine the levels of the different Aβ species produced (Takami et al, 2009). Thus, the true activity of γ-secretase is defined by the amounts of tri- and tetrapeptides released, but not by the amounts of Aβ species produced. Of note, the most abundant species Aβ40 is derived not from Aβ42, but from Aβ43. Also Aβ38 is derived mainly from Aβ42 (Fig 1). The longer Aβs in cerebrospinal fluid (CSF) including Aβ49 and 46 as well as Aβ48 and 45 must be generated at negligible levels, but may neither be secreted to the interstitial fluid (ISF) nor recruited to CSF. This suggests that the status of brain, and possibly neuronal, γ-secretase could be accurately assessed by measuring all four Aβ species generated by the two product lines of γ-secretase.

Using enzyme-linked immunosorbent assays (ELISAs), we quantified Aβ40 and 43 and Aβ38 and 42 in CSF samples from control subjects and mild cognitive impairment (MCI)/AD patients. The CSF concentrations of Aβ43 and Aβ42 were found to be significantly lower in MCI/AD compared with controls. The ratio of Aβ38/42, which represents the ratio of product/precursor and thus the cleavage efficiency of Aβ42, was plotted against the ratio of Aβ40/43, which represents the ratio of product/precursor in the other product line and thus the cleavage efficiency of Aβ43. The ratio of Aβ38/42 was largely proportional to that of Aβ40/43, indicating that the two cleavage processes are tightly coupled, but both were generally higher in MCI/AD patients compared to control subjects These results

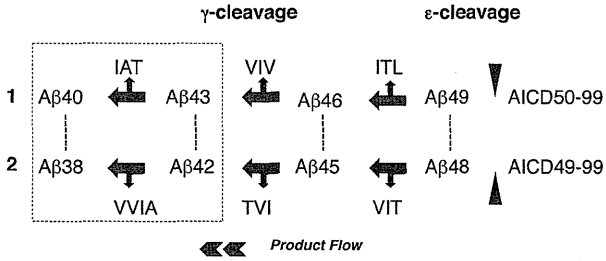

Figure 1. Generation of Aβs through stepwise processing of βCTF. At the first step, βCTF is cleaved at the membrane-cytoplasmic boundary (ε-cleavage), producing AICD (APP intracellular domain) 50–99 and 49–99. Counterparts Aβ49 and 48 in turn are cleaved in a stepwise fashion, releasing tri- and tetrapeptides. One product line converts Aβ49 mostly to Aβ40 via Aβ46 and Aβ43. The other product line converts Aβ48 to Aβ38 via Aβ45 and Aβ42. It should be noted that the differences between the amounts of released tri- or tetrapeptide determine the amounts of Aβs produced. Broken lines indicate corresponding Aβs on the two product lines.

suggest that the activity of brain γ-secretase in MCI/AD is enhanced at the conversion of Aβ43 to Aβ40 and Aβ42 to Aβ38, which would result in significantly lower CSF concentrations of Aβ42 and 43. In support of this hypothesis, the activities of raft-associated γ-secretase from control and MCI/AD brains were found to be significantly different: although the total Aβ production was similar, the γ-secretase in MCI/AD brains produced significantly larger ratios of Aβ40/43 and Aβ38/42 than the enzyme in control brains. This raises the possibility that lower CSF levels of Aβ42 and 43 simply reflect the altered γ-secretase activity in the MCI/AD-affected brains.

RESULTS

The CSF concentrations of Aβs were in the following order: Aβ40 > Aβ38 > Aβ42 ≫ Aβ43 in all CSF samples examined (Table 1 and Supporting Information Fig S2A). The relative amounts of Aβs were constant across the samples: Aβ38:40 ratio in CSF was ~1:3, and Aβ42:43 ratio was ~10:1. The CSF

Table 1. Subject characteristics and CSF concentrations of Aβs

	Control	MCI	AD	ANOVA ***p-value
Age (years)	74.9 ± 7.5	72.5 ± 6.6	72.3 ± 8.2	
N (male/female)	21 (10/11)	19 (7/12)	24 (7/17)	
MMSE score	28.7 ± 1.9	25.7 ± 2.6	19.6 ± 3.3	
ApoE ε4	3 (14.3%)	10 (52.6%) [a]	14 (58.6%) [a]	
Aβ38 (pM)	594.5 ± 286.3	669.4 ± 247.6	760.57 ± 269.4	
Ln(Aβ38)	6.28 ± 0.46	6.44 ± 0.38	6.56 ± 0.41	NS
Aβ40 (pM)	1607.9 ± 712.9	1939.5 ± 698.0	2292.6 ± 799.6	
Ln(Aβ40)	7.28 ± 0.47	7.51 ± 0.38	7.68 ± 0.35	0.007
Aβ42 (pM)	133.1 ± 53.4	83.2 ± 49.4**	90.3 ± 40.1 [a]	
Ln(Aβ42)	4.80 ± 0.47	4.25 ± 0.60	4.40 ± 0.47	0.004
Aβ43 (pM)	11.8 ± 5.7	6.8 ± 5.6**	7.0 ± 4.6**	
Ln(Aβ43)	2.32 ± 0.60	1.59 ± 0.86	1.76 ± 0.62	0.004

[a]2 MCI subjects were homozygous for ε4, while 4 AD subjects were homozygous for the allele.
**$p < 0.05$; Dunnett's *t*-test after log-transformation for comparing between control and MCI or AD.
***p-value of analysis of variance after log-transformation.

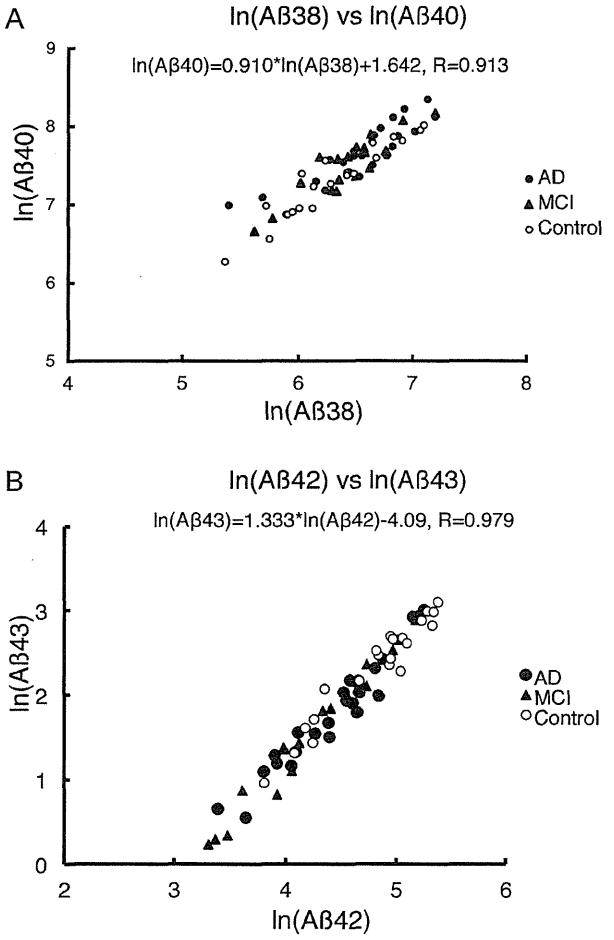

Figure 2. Relationships between the levels of Aβ40 and 38, and between those of Aβ43 and 42 in CSF from controls and MCI/AD patients.

A. The levels of ln(Aβ40) were proportional to those of ln(Aβ38) ($\ln(A\beta40) = 0.910 \times \ln(A\beta38) + 1.642$, $R = 0.913$).

B. The levels of ln(Aβ43) were proportional to those of ln(Aβ42) ($\ln(A\beta43) = 1.333 \times \ln(A\beta42) - 4.09$, $R = 0.979$). It should be noted that the levels of both ln(Aβ42) and ln(Aβ43) in MCI [filled triangle ($n = 19$)]/AD [filled circle ($n = 24$)] are lower than those in controls [open circles ($n = 21$)].

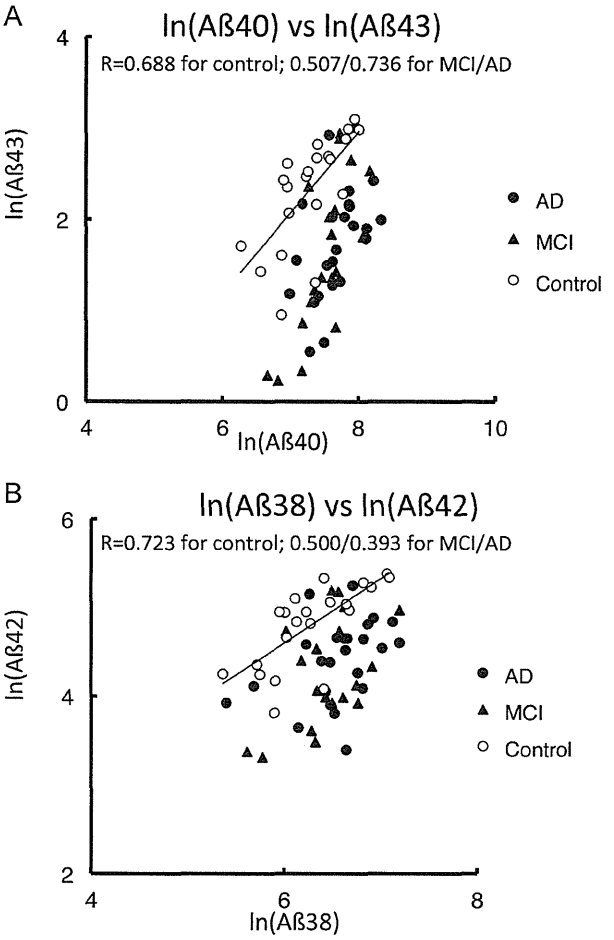

Figure 3. Relationships between the levels of Aβ43 and 40, and between those of Aβ42 and 38 in CSF from controls (open circles) and MCI (closed triangle)/AD patients (closed circle).

A. The levels of ln(Aβ43) correlate with those of ln(Aβ40) within controls ($R = 0.688$), and barely within MCI/AD subjects ($R = 0.507/0.736$). The plots for MCI/AD were located below the regression line for control ($p < 0.001$, ANOVA).

B. The levels of Aβ42 correlate with those of Aβ38 within controls ($R = 0.723$), and barely within MCI/AD ($R = 0.500/0.393$). The plots for MCI/AD were situated below the regression line for controls ($p < 0.001$, ANOVA).

concentrations of Aβ40 were significantly increased in AD compared to control (Table 1; $p < 0.05$, Dunnett's t-test). Additionally, the CSF concentrations of Aβ38 tended to be increased in AD patients compared to controls. In contrast, those of Aβ42 and 43 were significantly decreased in MCI/AD compared to controls ($p < 0.05$, Dunnett's t-test). Interestingly, as reported previously (Schoonenboom et al, 2005), the CSF concentrations of Aβ40 and Aβ38 were proportional to each other in all subjects [Fig 2A; $\ln(A\beta40) = 0.910 \times \ln(A\beta38) + 1.642$, $R = 0.913$, where ln(Aβ40) is the logarithm of Aβ40], even in MCI/AD cases. This was despite the fact that these species are derived from and the final products of the two different product lines of γ-secretase activity (Fig 1; Takami et al, 2009). In other words, the amounts of products in the third step of cleavage were strictly proportional to each other across the product lines.

Aβ42 and Aβ43 are produced by the second cleavage step of each product line. Like Aβ40 and Aβ38, the CSF concentrations of Aβ42 and Aβ43 are also proportional to each other in controls and in MCI/AD patients [Fig 2B; $\ln(A\beta43) = 1.333 \times \ln(A\beta42) - 4.09$, $R = 0.979$]. On the other hand, the levels of Aβ43 and Aβ40 (a precursor and its product) were correlated in control [Fig 3A; $\ln(A\beta43) = 0.884 \times \ln(A\beta40) - 4.118$, $R = 0.688$] and in MCI/AD subjects ($R = 0.507/0.736$ for MCI/AD, respectively) but the MCI/AD values were located below the regression line for controls and thus provided lower Aβ43 measures compared with controls for a given Aβ40 measure (Fig 3A; $p < 0.001$, analysis of variance, ANOVA). Conversely,

for a given Aβ43 value, the plot provided a higher Aβ40 measure in MCI/AD cases. There was a similar situation for the levels of Aβ42 and Aβ38. The levels of Aβ42 and Aβ38 were correlated each other in control subjects [Fig 3B; $\ln(A\beta42) = 0.724 \times \ln(A\beta38) + 0.251$, $R = 0.723$], but barely in MCI/AD ($R = 0.500$ for MCI; 0.393 for AD), and the MCI/AD plots were situated below the regression line for controls ($p < 0.001$, ANOVA). For a given Aβ42 value, the plot provided a higher Aβ38 measure in MCI/AD compared with controls.

These lower concentrations of Aβ42 appeared to be compensated with higher concentrations of Aβ38 as the levels of ln(Aβ38 + Aβ42) did not vary even in MCI/AD ($p = 0.293$, ANOVA). Thus, this points to the possibility that more Aβ42 and Aβ43 are converted to Aβ38 and Aβ40, respectively, in MCI/AD brains. According to numerical simulation based on the stepwise processing model, as the levels of βCTF decline to null, the levels of Aβ43 and 42 decrease and the ratios of Aβ40/43 and Aβ38/42 increase (unpublished observation). However, this situation can be excluded as the mechanism for lower concentrations of Aβ42 and 43, because the levels of βCTF have never been reported to be reduced in AD brains nor in plaque-forming Tg2576 mice that show lower CSF Aβ42 concentrations (Kawarabayashi et al, 2001). Thus, it is reasonable to suspect that the final cleavage steps from Aβ43 mostly to 40 and from Aβ42 to 38 are significantly enhanced in parallel (increases in released tri- and tetrapeptides) in brains affected by MCI/AD compared with controls (Fig 1).

This relationship in γ-secretase cleavage becomes clearer by plotting the product/precursor ratio representing cleavage efficiency at the step from Aβ42 to 38 (Aβ38/42) against that representing the cleavage efficiency at the step from Aβ43 to 40 (Aβ40/43) (Fig 4). The 'apparent' cleavage efficiency of Aβ43 was approximately 40-fold larger than that of Aβ42. The two ratios in CSF samples from MCI/AD and control subjects were largely proportional to each other, indicating that the corresponding cleavage processes in the two lines are tightly coupled (Fig 4). All plots were situated on a distinct line [$\ln(A\beta38/42) = 0.748 \times \ln(A\beta40/43) - 2.244$, $R = 0.936$] and its close surroundings. An increase in the cleavage from Aβ43 to 40 (*i.e.* more Aβ43 is converted to Aβ40) accompanied an increase in the cleavage from Aβ42 to 38 and *vice versa*, although the mechanism underlying this coupling between the two product lines remains unknown. This reminds us of the 'NSAID effect' in the 3-([3-cholamidopropyl]dimetylammonio)-2-hydroxy-1-propanesulfonate (CHAPSO)-reconstituted γ-secretase system (Takami et al, 2009; Weggen et al, 2001) in which the addition of sulindac sulfide to the γ-secretase reaction mixture, as expected, significantly suppressed Aβ42 production and increased Aβ38 production presumably by increasing the amounts of released tetrapeptide (VVIA) (Takami et al, 2009) and other peptides.

Most importantly, this graph provides a clear distinction between the control and MCI/AD groups (Fig 4; Aβ40/43 for MCI/AD *vs.* control, $p = 0.000$; Aβ38/42 for MCI/AD *vs.* control, $p = 0.000$; ANOVA, followed by Dunnett's *t*-test). The control values plotted close to the origin, whereas those for MCI/AD patients were distant from the origin along the line [$\ln(A\beta38/42) = 0.748 \times \ln(A\beta40/43) - 2.244$, $R = 0.936$]. It is also of note

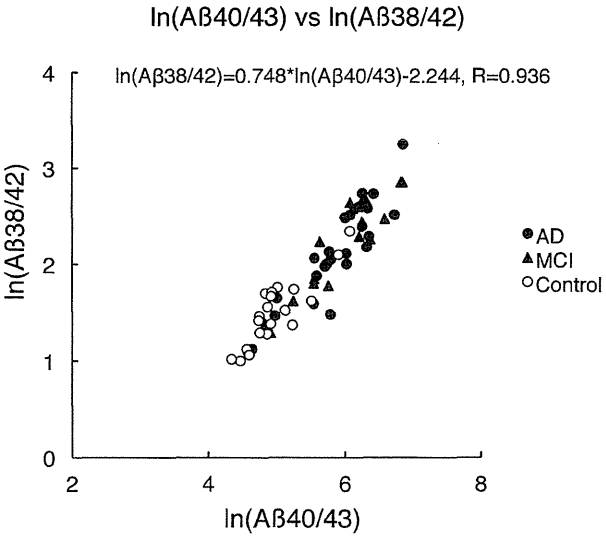

Figure 4. Ln(Aβ40/43) *versus* ln(Aβ38/42) plot. The ratios represent the cleavage efficiency at the final step of each line. Both ratios are largely proportional to each other ($y = 0.748 \times -2.244$, $R = 0.936$) and plots are located on the line and its close surroundings. This plot clearly distinguishes between control subjects and MCI/AD patients (Aβ40/43 for MCI *vs.* control, $p = 0.000$; Aβ38/42 for MCI *vs.* control, $p = 0.000$; ANOVA, followed by Dunnett's *t*-test). Control plots [open circles ($n = 21$)] are located close to the origin and MCI/AD plots [closed triangles ($n = 19$) and closed circles ($n = 24$), respectively] are a little distant from the origin.

that there was no significant difference between MCI and AD patients (Fig 4; Aβ40/43 for AD *vs.* MCI, $p = 1.000$; Aβ38/42 for AD *vs.* MCI, $p = 1.000$; Bonferroni's *t*-test). Two control values were a little farther from the origin, which may suggest that these subjects already have latent Aβ deposition or are in the preclinical AD stage. Additionally, we examined quite a small number of CSF samples from presenilin (PS) 1-mutated (symptomatic) familial AD (FAD) patients (T116N, L173F, G209R, L286V and L381V). Out of the three FAD cases near the regression line, two (T116N and L286V) were distant from the origin like sporadic AD cases and one (L381V) was closer to the origin than controls (both Aβ42/43 levels were lower than control; unpublished data). The remaining two (G209R and L173F) were extremely displaced from the line. Thus, a larger number of FAD cases are needed to give an appropriate explanation for their unusual characteristics in the plot, and the alteration of CSF Aβs shown above seems to be applicable only for sporadic AD.

Altogether, in MCI/AD, more Aβ42 and 43 are processed to Aβ38 and 40, respectively, than in controls. Even in MCI/AD, strict relationships are maintained between the levels of Aβ42 and Aβ43, and between those of Aβ38 and Aβ40 as seen in controls, which are predicted by the stepwise processing kinetics (unpublished observation). Thus, our observations suggest that lower CSF concentrations of Aβ42 and 43 and presumably higher CSF concentrations of Aβ38 and 40 are the consequence of altered γ-secretase activity in brain rather than the effect of preferential deposition of the two longer Aβ species (Aβ42 and 43) in senile plaques, which would not have maintained such strict relationships between the four Aβ species in CSF.

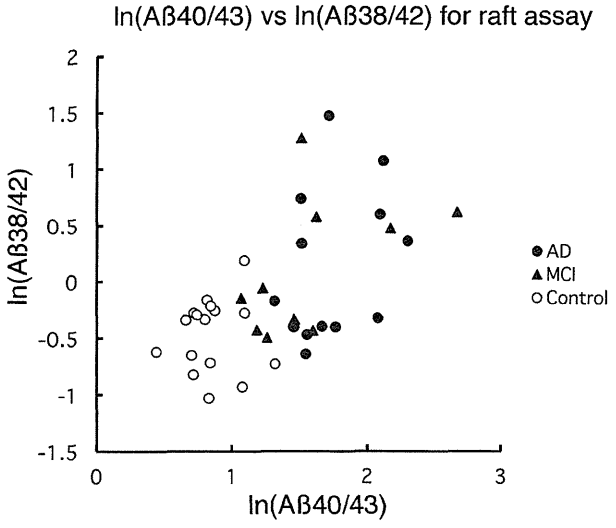

Figure 5. Ln(Aβ40/43) *versus* ln(Aβ38/42) plot based on direct quantification of raft-associated γ-secretase activity. The raft-associated γ-secretase prepared from control and MCI/AD brain specimens was incubated with βCTF for 2 h at 37°C (see Materials and Methods Section). Produced Aβs were quantified by Western blotting using specific antibodies. This plot distinguishes between control subjects and MCI/AD patients (Aβ40/43 for control *vs.* MCI/AD, $p < 0.001$; Aβ38/42 for control *vs.* MCI/AD, $p = 0.001$; Welch's *t*-test). MCI/AD plots [closed triangles ($n = 10$) and closed circles ($n = 13$), respectively] are as a whole a little distant from the origin, whereas control plots [open circles ($n = 16$)] are close to the origin.

To further test our hypothesis, we directly measured γ-secretase activities associated with lipid rafts isolated from AD, MCI and control cortices (Brodmann areas 9–11). For definite confirmation of the Aβ species, the reaction mixtures were subjected to quantitative Western blotting using specific antibodies rather than ELISA. At time 0, deposited Aβ42/43 species were detected in rafts from MCI/AD brains but not in control specimen (Supporting Information Fig S3). The amounts of ln(Aβ38 + Aβ42), which reflect the total capacity of the Aβ38/42-producing line, did not vary between AD, MCI and controls (Supporting Information Fig S4; $p = 0.969$, ANOVA). Thus, the gross activities of raft γ-secretase were comparable among the three groups. However, the plotted values for Aβ40/43 *versus* Aβ38/42 are divided into two groups: MCI/AD and controls (Fig 5; Aβ40/43 for control *vs.* MCI/AD, $p < 0.001$; Aβ38/42 for control *vs.* MCI/AD, $p = 0.001$; Welch's *t*-test) in the same way as those derived from CSF (Fig 4). It is notable that Figs. 4 and 5 are based on different methods, ELISA and Western blotting, respectively, but give similar results. There were no significant differences between MCI and AD specimen, although MCI patients (91 ± 4.9-year-old) were older than controls (77 ± 6.5-year-old) or AD patients (80 ± 5.0-year-old) (Aβ40/43 for MCI *vs.* AD, $p = 0.342$; Aβ38/42 for MCI *vs.* AD, $p = 0.911$). There were similar significant differences between control *versus* AD in the groups of which the ages were not significantly different (Aβ40/43 for control *vs.* AD, $p < 0.001$; Aβ38/42 for control *vs.* AD, $p = 0.03$).

DISCUSSION

Here, we assume that (i) Aβs in CSF are produced exclusively by γ-secretase in the brain, possibly in neurons; and (ii) Aβs in CSF are in the steady state. With these assumptions, the combined measurement of four Aβ species in CSF should predict the activity of γ-secretase in the brain. Here, the alterations in the γ-secretase activities do not mean the gross activity, *i.e.* total Aβ production, but the cleavage efficiency of the intermediates, Aβ42 and Aβ43.

In the present study, we quantified in CSF the four Aβ species, Aβ38/42 and Aβ40/43, but the Western blotting indicated the presence of additional Aβ species, Aβ37 and 39, in CSF (Supporting Information Fig S2). At present, we cannot exclude the possibility that a certain carboxyl terminus-specific protease(s) in CSF acts on the pre-existing Aβ species and converts them to Aβ37 and 39 (Zou et al, 2007). However, according to our unpublished data (Takami et al, unpublished observations), it is plausible that Aβ37 is derived from Aβ40, whereas Aβ39 is derived from Aβ42. Even if so, these pathways are very minor (~20–100-fold less) compared to the two major pathways, Aβ42 to Aβ38, and Aβ43 to Aβ40, when assessed by a reconstituted system (Takami et al, 2009). Thus, such strict relationships between four Aβs may have been relatively independent of Aβ37 and 39. The detailed relationship between all Aβs in the CSF awaits further quantification of the additional two Aβ species.

Currently, we do not know why the observation that Aβ40 is higher in MCI/AD CSF has so far not been reported except a recent paper (Simonsen et al, 2007). In fact, some of us previously reported no significant differences in CSF Aβ40 between AD and control subjects using a different ELISA (Shoji et al, 1998). It may be notable that we used newly constructed ELISA for Aβ40 based on a different set of monoclonal antibodies and thus, those discrepancies may come from the different antibody/epitope combination used for ELISA and/or different assay methods. In particular, it should be noted that all ELISAs used here detect Aβ1-x only, but not amino-terminally truncated forms. In this context, the ratio of Aβ40/43 appears to be more informative to discriminate between control and MCI/AD than the absolute levels of Aβ40 alone (Table 1 and Fig 5). It is possible that even if Aβ40 is not different between control and MCI/AD, the ratio Aβ40/43 could discriminate them.

We are the first to measure CSF Aβ43 using ELISA. The CSF concentrations of Aβ43 are 10-fold less than those of Aβ42. Nevertheless, the specificity of the newly constructed ELISA made the quantification of accurate levels of Aβ43 possible (Supporting Information Fig S1). Regarding the Aβ43 measures, we observed that its behaviour is entirely similar to that of Aβ42 in MCI/AD. Our preliminary observations using immunocytochemistry and ELISA quantification strongly suggest that Aβ43 deposits in aged human brains at the same time as Aβ42 (unpublished observations). Furthermore, Saido and colleagues have only recently reported that a PS1 R278I mutation in mice (heterozygous) caused an elevation of Aβ43 and its early and pronounced accumulation in the brain (Saito et al, 2011). It is possible that the cleavage of βCTF by this R278I γ-secretase may

be profoundly suppressed in the third cleavage step of the product line 1 (see Fig 1), which would result in negligible levels of Aβ40 and unusually high levels of Aβ43 (Nakaya et al, 2005). These results suggest that the role of Aβ43 should be reconsidered for the initiation of β-amyloid deposition and thus in AD pathogenesis.

Lower CSF concentrations of Aβ42 and 43 are not exclusively limited to MCI/AD. For example, similar low concentrations of Aβ42 and 43 were found in the CSF from eight patients with idiopathic normal pressure hydrocephalus (iNPH) (Aβ42, 76.3 ± 37.3 pM, $p = 0.012$ compared to controls: Aβ43, 5.2 ± 2.9 pM, $n = 8$, $p = 0.004$ compared to controls: Bonferroni's *t*-test; Silverberg et al, 2003). Thus, lower CSF concentrations of Aβ42 and 43 alone were unable to distinguish between iNPH and MCI/AD, and further, it is claimed that the former is often associated with abundant senile plaques, raising the possibility that Aβ deposition is enhanced by iNPH (Silverberg et al, 2003). However, when their partners Aβ38 and 40 were measured in CSF, both were found not to be significantly increased in iNPH (Aβ38, 459.2 ± 138.5 pM, $p = 0.484$ compared to controls; Aβ40, 1094.4 ± 375.3 pM, $n = 8$, $p = 0.103$ compared to controls; Table 1) in sharp contrast to MCI/AD indicating that the cleavage in iNPH at the steps from Aβ43 to 40 and from Aβ42 to 38 is not enhanced as it is in MCI/AD. Thus, it may be that the dilution effect elicited by ventricular enlargement would be the cause of lower CSF Aβ42 and 43 found in iNPH.

Currently, we do not know the mechanism behind the altered activity of brain γ-secretase in MCI/AD (Fig 4). First, it is of note that rafts prepared from MCI/AD brains but never from control brains at SP stage 0/A accumulated Aβ42 and Aβ43 (Supporting Information Fig S3; Oshima et al, 2001). It is possible that raft-deposited Aβ42/43 could induce a change in the γ-secretase activity, although the extent of the alteration in the activity appears not to be related to the extent of accumulation (unpublished observation). In this regard, it is of interest to note that Tg2576 mice, the best characterized AD animal model, shows reduced levels of Aβ42 in plasma as well as in CSF at the initial stage of Aβ deposition (Kawarabayashi et al, 2001). If the assumption here is correct, this may suggest that γ-secretase that produces plasma Aβs could also be altered. However, thus far, we have failed to replicate significantly lower Aβ42 levels or Aβ42/Aβ40 ratios in plasma from AD patients.

Second, there could be heterogenous populations of γ-secretase complexes that have distinct activities due to subtle differences in their components. γ-Secretase is a complex of four membrane proteins including PS, nicastrin (NCT), anterior pharynx defective 1 (Aph1) and presenilin enhancer 2 (Pen 2) (Takasugi et al, 2003). Aph 1 has three isoforms, and each can assemble active γ-secretase together with other components (Serneels et al, 2009). NCT, a glycoprotein, is present in immature and mature forms (Yang et al, 2002). The abundance of these heterogenous populations of proteins in the brain is probably under strict control. During MCI/AD, a certain population could replace other populations of γ-secretase and thus may show a distinct activity as a whole.

The data shown here represent only a cross-sectional study, but our keen interest is how the CSF levels of the four Aβ species would shift during the longitudinal course in an individual who is going to develop sporadic AD. Does one have any period during life when Aβ42 and 43 are at higher levels in CSF, and thus the ratios of Aβ38/42 and Aβ40/43 are smaller? At this period when the final cleavage steps of γ-secretase would be suppressed, the ISF concentrations of Aβ43 and 42 would increase, which would start or promote their aggregation in the brain parenchyma. If so, during life span, the individual's plot would move down along the regression line and move up as senile plaques accumulate, and the individual would eventually develop sporadic AD. However, thus far the period when there are increases in CSF Aβ42/43 has never been reported for sporadic AD. Nor has it been reported for asymptomatic FAD carriers (Ringman et al, 2008), whereas their plasma is known to contain higher levels (and percent) of Aβ42 (Kosaka et al, 1997; Ringman et al, 2008; Scheuner et al, 1996). It is likely that the stage of normal cognition and Aβ accumulation already accompanies reduced CSF Aβ42. If so, the alterations of γ-secretase should continue on for decades. Most interestingly, this alteration of CSF Aβ regulation seems to be planned to prevent further accumulation of Aβ42 and 43 in the brain.

However, Hong et al (2011) have recently shown, using *in vivo* microdialysis to measure ISF Aβ in APP transgenic mice, that the increasing parenchymal Aβ is closely correlated with decreasing ISF Aβ, suggesting that produced Aβ42 is preferentially incorporated into existing plaque-Aβ. This is a prevailing way of the interpretation of the data. Another way of the interpretation of data would be that during aging from 3 to 24 months, γ-secretase activity becomes altered and produces decreasing amounts of Aβ but with an increasing ratio of Aβ38/42 (and Aβ40/43). It is worth to mention that produced Aβ42 (but not Aβ40) appears to be selectively bound to rafts (from CHO cells) after long incubation (>4 h; Wada et al, unpublished observation). Also of note is that we quantified the total (free and bound) Aβ produced by an *in vitro* reconstituted system (Fig 5). What is claimed here is that decreased levels of CSF Aβ42 are largely due to alterations of γ-secretase activity rather than due to selective deposition of Aβ42 in preexisting plaques. What proportions of decreased ISF (CSF) Aβ42 levels would be contributed to by altered γ-secretase activity and selective deposition of Aβ42/43 to parenchymal plaques awaits future studies.

Finally, our observation has therapeutic implication. As shown elsewhere and here above, if Aβ42 is the culprit for MCI/AD, non-steroidal anti-inflammatory drugs (NSAIDs) would have been quite a reasonable therapeutic compound, which enhances cleavage at the third step in the stepwise processing, leading to lower levels of Aβ42 without greatly interfering with the Aβ bulk flow (Weggen et al, 2001). This sharply contrasts with some of the γ-secretase inhibitors currently under development and in clinical trial, which block the Aβ bulk flow. However, the present study raises the possibility that even if NSAIDs are administered, the expected beneficial effect could be minimal in MCI/AD patients, because in these patient brains, γ-secretase is already shifted to an NSAID-like effect.

MATERIALS AND METHODS

Subjects

Cerebrospinal fluid samples from 24 AD patients (mild to moderate AD; 50–86 years old), 19 MCI patients (57–82 years old) and 21 control subjects (61–89 years old) were collected (see Table 1) at Department of Neurology, Hirosaki University Hospital and at Department of Geriatrics and Gerontology, Tohoku University Hospital, and at Department of Neurology, Niigata University Hospital. The CSF samples from (symptomatic) 5 FAD (mPS1) patients (T116N, L173F, G209R, L286V and L381V) were from Niigata University Hospital. Probable AD cases met the criteria of the National Institute of Neurological and Communicative Disorders and Stroke–Alzheimer's Disease and Related Disorders (NINCDS-ADRDA) (Kuwano et al, 2006; McKhann et al, 1984). Additional diagnostic procedures included magnetic resonance imaging. Dementia severity was evaluated by the Mini-Mental State Examination (MMSE). Diagnosis of MCI was made according to the published criteria (Winblad et al, 2004). Diagnosis of iNPH was made according to the guideline issued by the Japanese Society of NPH (Ishikawa et al, 2008). Controls who had no sign of dementia and lived in an unassisted manner in the local community were recruited. All individuals included in this study were Japanese and 24 AD patients examined here were judged to have sporadic AD because of negative family history. This study was approved by the ethics committee at each hospital or institute.

Human cortical specimens for quantification of raft-associated γ-secretase activity were obtained from those brains that were removed, processed and placed in −80°C within 12 h postmortem [Patients were placed in a cold (4°C) room within 2 h after death] at the Brain Bank at Tokyo Metropolitan Institute of Gerontology. For all the brains registered at the bank we obtained written informed consents for their use for medical research from patient or patient's family. Each brain specimen (~0.5 g) were taken from Brodmann areas 9–11 of 13 AD patients [80 ± 5.0 years of age, Braak NFT stage > IV, SP stage = C (retrospective) CDR ≫ 1], 10 MCI patients (91 ± 4.9 years of age, Braak NFT stage < IV, SP stage < C, CDR = 0.5) and 16 controls (77 ± 6.5 years of age, Braak NFT stage < I, SP stage = 0/A, CDR = 0) (Adachi et al, 2010; Li et al, 1997).

Cerebrospinal fluid analysis

Cerebrospinal fluid (10–15 ml) was collected in a polypropylene or polystyrene tube and gently inverted. After brief centrifugation CSF was aliquotized to polypropylene tubes (0.25–0.5 ml), which were kept at −80°C until use. In our experience, Aβ42 (possibly, other Aβ species too) are readily absorbed even to polypropylene tubes (~20% per new exposure, as shown by Luminex xMAP quantification), and repeated aliquotization to new tubes may cause profoundly lower measures of Aβs (Tsukie and Kuwano, unpublished data, 2010). This may partly explain why absolute levels of Aβs in CSF greatly vary among laboratories, whereas their relative ratios (*e.g.* Aβ42/40) seem to be roughly consistent. The CSF concentrations of Aβ38, 40 and 42 were quantified using commercially available ELISA kits (Cat no. 27717, 27718 and 27712, respectively, IBL, Gunma, Japan). To measure Aβ43, anti-Aβ43 polyclonal antibody as a capture antibody was combined with amino terminus-specific antibody (82E1) (Cat no. 10323, IBL, Gunma, Japan) as a detector antibody. The detection limit of Aβ43 quantified by the ELISA was 0.78 pM (data not shown). Thus all ELISAs used here detect Aβ1-x, but not amino-terminally truncated Aβs. The specificities of ELISAs are provided in Supporting Information Fig S1.

CSF immunoprecipitation and Western blotting

When required, CSF Aβs were immunoprecipitated with protein G-sepharose conjugated with 82E1 at 4°C by keeping a container in gentle rotation overnight. The mixture was centrifuged at 10,000×g for 5 min, and resultant pellets were then washed twice with phosphate-buffered saline. The washed beads were suspended with the Laemmli sample buffer for SDS–polyacrylamide gel electrophoresis (SDS–PAGE). The immunoprecipitated Aβs were separated on Tris/Tricine/8 M urea gels (Kakuda et al, 2006), followed by Western blotting using 82E1. To immunodetect Aβ42 and Aβ43, Aβ42 monoclonal antibody (44A3, IBL) and Aβ43 polyclonal antibody (IBL) were used (Supporting Information Fig S3).

Numerical simulation based on the stepwise processing model of γ-secretase

The temporal profiles for the ratios of Aβ40/43 and Aβ38/42 were simulated based on the stepwise processing model. Parameters including rate constants were set to fit maximally the temporal profile of the cleaving activity in the reconstituted γ-secretase system (Takami et al, 2009).

We set the condition that βCTF substrate is supplied steadily from the external source. When βCTF supply is balanced roughly in the order with γ-secretase processing rate, the stepwise-processing model was found to have the two successive steady states, with each accompanying linear changes in [ES] or [S] concentrations. The first steady state is just after the initial transition period that corresponds to the acute saturation phase of γ-secretase with βCTF. The second steady state is associated with the constant concentrations of the enzyme/substrate complex except ES38 and ES40. Because these steady states kept the ratios of Aβ38/Aβ40 and Aβ42/Aβ43 constant, the simulation was quite consistent with the CSF data.

Quantification of human brain raft-associated γ-secretase activity

Since γ-secretase is thought to be concentrated in rafts (Hur et al, 2008; Wada et al, 2003), we measured raft-associated γ-secretase activity rather than CHAPSO-solubilized activity. Rafts were prepared from human brains which were frozen within 12 h postmortem, as previously described (Oshima et al, 2001; Wada et al, 2003) with some modifications. We do not know exactly whether the γ-secretase activity depends upon the sampling site. In our hands, there appear no large differences in the activity among the sampled sites in a given prefrontal slice. No significant differences in the activity were noted between outer and inner layer of the cortex. After carefully removing leptomeninges and blood vessels, small (<0.5 g) blocks from prefrontal cortices (Brodmann areas 9–11) were homogenized in ~10 volumes of 10% sucrose in MES-buffered saline (25 mM MES, pH 6.5, and 150 mM NaCl) containing 1% CHAPSO and various protease inhibitors. The homogenate was adjusted to 40% sucrose by the addition of an equal volume of 70% sucrose in MES-buffered saline, placed at the bottom of an ultracentrifuge tube, and overlaid with 4 ml of 35% sucrose and finally with 4 ml of 5% sucrose in MES-buffered saline. The discontinuous gradient was centrifuged at 39,000 rpm for 20 h at 4°C on a SW 41 Ti rotor (Beckman, Palo

The paper explained

PROBLEM:

Alzheimer's disease is a devastating form of progressive dementia, in which senile plaques composed of Aβ form in the brain. Different species of Aβ are derived from APP through sequential cleavage by β- and γ-secretases and can be detected in the CSF of patients. These can serve as markers for the disease.

RESULTS:

We investigated why CSF concentrations of Aβ42 are lower in MCI and AD patients. We suggest that this is not because Aβ42/43 is selectively deposited in the brain, but because γ-secretase activity is altered in AD brain: more Aβ42 and Aβ43 are converted to Aβ40 and Aβ38, respectively, resulting in lower Aβ42 and Aβ43 in CSF.

IMPACT:

Our results predict that γ-secretase modulators would have only limited efficacy in treatment of AD patients, because Aβ42/43 production by γ-secretase is already shifted towards reduced levels in AD brain.

Alto, CA). An interface of 5%/35% sucrose (fraction 2) was carefully collected (referred to as raft fraction). Raft fractions were recentrifuged after dilution with buffer C (20 mM PIPES, pH 7.0, 250 mM sucrose and 1 mM EGTA). The resultant pellet was washed twice and resuspended with buffer C, which was kept at −80°C until use.

As the method of measuring the raft γ-secretase activity was not yet established, we first determined the assay conditions. The incubation of raft fraction with βCTF generated exactly the same tri- and tetrapeptides we previously observed in the detergent-soluble γ-secretase assay system (Takami et al, unpublished observation). This suggests that the cleavage by raft-associated γ-secretase proceeds in the identical manner as by CHAPSO-reconstituted γ-secretase (Takami et al, 2009). In our hands, preexisting βCTF bound in rafts generated only negligible amounts of Aβs, and their generation was dependent exclusively on exogenously added βCTF. Thus, we concluded that the addition of βCTF to raft fraction make possible to measure the raft-associated γ-secretase activity, although we do not know how the exogenously added βCTF is integrated into raft, gets access to and is degraded by raft-embedded γ-secretase. Using this assay method, the activities of raft-associated γ-secretase in human brains were found to be only a little affected postmortem, when compared with that prepared from fresh rat brains. A progressive decline in the activity was barely detectable from 4 to 17 h postmortem. The discrepancy in the postmortem decay between our and the previous data (Hur et al, 2008) would be ascribed to the assay method: the latter are based on the activity measured by using endogenous (raft-bound) substrate that is also susceptible to proteolytic degradation (Hur et al, 2008).

Each raft fraction, adjusted to 100 μg/ml in protein concentration, was incubated with 200 nM C99FLAG for 2 h at 37°C (Kakuda et al, 2006). The produced Aβs were separated on SDS–PAGE, and subjected to quantitative Western blotting, using specific antibodies, 3B1 for Aβ38, BA27 for Aβ40, 44A3 for Aβ42 and anti-Aβ43 polyclonal for Aβ43.

Statistical analysis

All statistical analyses were performed using SPSS version 14.0. The results were expressed as means ± standard deviations. Because data transformations were required to achieve normally distributed data, all analyses including Aβ38, Aβ40, Aβ42 and Aβ43 were performed after a logarithmic transformation. Pearson's correlation coefficients were calculated to indicate the strength of the linear relationship between two variables. An ANOVA was used to test the equality of mean values of continuous variables among three groups, that is control, MCI and AD. Multiple comparisons were done by Dunnett's *t*-test, Bonferroni's *t*-test and Welch's *t*-test between control and MCI/AD, and among three groups, respectively. A two-tailed *p*-value of <0.05 was considered to be statistically significant.

Author contributions

NK, MT, KN, YI: measurement of raft-associated γ-secretase activity in human brains, LC-MS/MS confirmation of released peptides, ELISA quantification of Aβ38, 40, 42 and 43 in CSF and tissue blocks, and experimental design of the present work; MS, HiA, KF, TI, and the Japanese Alzheimer's Disease Neuroimaging Initiative: collection of CSF samples from controls, MCI/AD patients; YH, MM, HaA: collection of CSF from iNPH patients; HY, SM, HH: Aβ immunocytochemistry of tissue sections from brains with various SP stages (Braak); KA: statistical analysis; RK: establishment of the appropriate Aβ quantification conditions; YN: simulation of the stepwise processing model.

Acknowledgements

We thank Dr. Haruhiko Akiyama, Department of Psychogeriatrics, Tokyo Institute of Psychiatry, Tokyo Metropolitan Organization for Medical Research, Tokyo, for the help in the initial phase of this study, and Dr. Takaomi C. Saido, RIKEN Brain Science Institute, for sharing the data on his R278I transgenic mice. Dr. Makoto Higuchi, Molecular Imaging Center, National Institute of Radiological Sciences, Chiba, kindly provided us with aged Tg2576 littermates. This project was supported by New Energy and Industrial Technology Development Organization in Japan (J-ADNI).

Supporting Information is available at EMBO Molecular Medicine online.

The authors declare that they have no conflict of interest.

References

Adachi T, Saito Y, Hatsuta H, Funabe S, Tokumaru AM, Ishii K, Arai T, Sawabe M, Kanemaru K, Miyashita A, *et al* (2010) Neuropathological asymmetry in argyrophilic grain disease. J Neuropathol Exp Neurol 69: 737-744

Hong S, Quintero-Monzon O, Ostaszewski BL, Podlisny DR, Cavanaugh WT, Yang T, Holtzman DM, Cirrito JR, Selkoe DJ (2011) Dynamic analysis of amyloid β-protein in behaving mice reveals opposing changes in ISF versus parenchymal Aβ during age-related plaque formation. J Neurosci 31: 15861-15869

Hur JY, Welander H, Behbahani H, Aoki M, Frånberg J, Winblad B, Frykman S, Tjernberg LO (2008) Active gamma-secretase is localized to detergent-resistant membranes in human brain. FEBS J 275: 1174-1187

Ishikawa M, Hashimoto M, Kuwana N, Mori E, Miyake H, Wachi A, Takeuchi T, Kazui H, Koyama H (2008) Guidelines for management of idiopathic normal pressure hydrocephalus. Neurol Med Chir (Tokyo) 48: S1-S23

Iwatsubo T, Odaka A, Suzuki N, Mizusawa H, Nukina N, Ihara Y (1994) Visualization of Aβ42(43) and Aβ40 in senile plaque with end-specific Aβ monoclonals: evidence that an initially deposited forms is Aβ42(43). Neuron 13: 45-53

Kakuda N, Funamoto S, Yagishita S, Takami M, Osawa S, Dohmae N, Ihara Y (2006) Equimolar production of amyloid β-protein and amyloid precursor protein intracellular domain from β-carboxyl-terminal fragment by γ-secretase. J Biol Chem 281: 14776-14786

Kawarabayashi T, Younkin LH, Saido TC, Shoji M, Ashe KH, Younkin SG (2001) Age-dependent changes in brain, CSF, and plasma amyloid (β) protein in the Tg2576 transgenic mouse model of Alzheimer's disease. J Neurosci 21: 372-381

Kosaka T, Imagawa M, Seki K, Arai H, Sasaki H, Tsuji S, Asami-Odaka A, Fukushima T, Imai K, Iwatsubo T (1997) The βAPP717 Alzheimer mutation increases the percentage of plasma amyloid-beta protein ending at Aβ42(43). Neurology 48: 741-745

Kuwano R, Miyashita A, Arai H, Asada T, Imagawa M, Shoji M, Higuchi S, Urakami K, Kakita A, Takahashi H, *et al* (2006) Dynamin-binding protein gene on chromosome 10q is associated with late-onset Alzheimer's disease. Hum Mol Genet 15: 2170-2182

Li G, Aryan M, Silverman JM, Haroutunian V, Perl DP, Birstein S, Lantz M, Marin DB, Mohs RC, Davis KL (1997) The validity of the family history method for identifying Alzheimer disease. Arch Neurol 54: 634-640

McKhann G, Drachman D, Folstein M, Katzman R, Price D, Stadlan EM (1984) Clinical diagnosis of Alzheimer's disease: report of the NINCDS-ADRDA Work Group under the auspices of Department of Health and Human Services Task Force on Alzheimer's Disease. Neurology 34: 939-944

Nakaya Y, Yamane T, Shiraishi H, Wang HQ, Matsubara E, Sato T, Dolios G, Wang R, De Strooper B, Shoji M, *et al* (2005) Random mutagenesis of presenilin-1 identifies novel mutants exclusively generating long amyloid β-peptides. J Biol Chem 280: 19070-19077

Oshima N, Morishima-Kawashima M, Yamaguchi H, Yoshimura M, Sugihara S, Khan K, Games D, Schenk D, Ihara Y (2001) Accumulation of amyloid beta-protein in the low-density membrane domain accurately reflects the extent of beta-amyloid deposition in the brain. Am J Pathol 158: 2209-2218

Qi-Takahara Y, Morishima-Kawashima M, Tanimura Y, Dolios G, Hirotani N, Horikoshi Y, Kametani F, Maeda M, Saiso TC, Wang R, *et al* (2005) Longer forms of amyloid β protein: implications for the mechanism of intramembrane cleavage by γ-secretase. J Neurosci 25: 436-445

Ringman JM, Younkin SG, Pratico D, Seltzer W, Cole GM, Geschwind DH, Rodriguez-Agudelo Y, Schaffer B, Fein J, Sokolow S, *et al* (2008) Biochemical markers in persons with preclinical familial Alzheimer disease. Neurology 71: 85-92

Saito T, Suemoto T, Brouwers N, Sleegers K, Funamoto S, Mihira N, Matsuba Y, Yamada K, Nilsson P, Takano J, *et al* (2011) Potent amyloidogenicity and pathogenicity of Aβ43. Nat Neurosci 14: 1023-1032

Scheuner D, Eckman C, Jensen M, Song X, Citron M, Suzuki N, Bird TD, Hardy J, Hutton M, Kukull W, *et al* (1996) Secreted amyloid β-protein similar to that in the senile plaques of Alzheimer's disease in increase in vivo by the presenilin 1 and 2 and APP mutations linked to familial Alzheimer's disease. Nat Med 2: 864-870

Schoonenboom NS, Mulder C, Van Kamp GJ, Mehta SP, Scheltens P, Blankenstein MA, Mehta PD (2005) Amyloid β 38, 40, and 42 species in cerebrospinal fluid: more of the same. Ann Neurol 58: 139-142

Selkoe DJ (2001) Alzheimer's disease: genes, proteins, and therapy. Physiol Rev 81: 741-766

Serneels L, Van Biervliet J, Craessaerts K, Dejaegere T, Horre K, Van Houtvin T, Esselmann H, Paul S, Schafer MK, Berezovska O, *et al* (2009) γ-Secretase heterogeneity in the Aph1 subunit: relevance for Alzheimer's disease. Science 324: 639-642

Shoji M, Matsubara E, Kanai M, Watanabe M, Nakamura T, Tomidokoro Y, Shizuka M, Wakabayashi K, Igeta Y, Ikeda Y, *et al* (1998) Combination assay of CSF tau, Aβ1–40 and Aβ 1–42(43) as a biochemical marker of Alzheimer's disease. J Neurol Sci 158: 134-140

Silverberg GD, Mayo M, Saul T, Rubenstein E, McGuire D (2003) Alzheimer's disease, normal-pressure hydrocephalus, and senescent changes in CSF circulatory physiology: a hypothesis. Lancet Neurol 2: 506-511

Simonsen AH, Hansson SF, Ruetschi U, McGuire J, Podust VN, Davies HA, Mehta P, Waldemar G, Zetterberg H, Andreasen N, *et al* (2007) Amyloid β1–40 quantification in CSF: comparison between chromatographic and immunochemical methods. Dement Geriatr Cogn Disord 23: 246-250

Takami M, Nagashima Y, Sano Y, Ishihara S, Morishima-Kawashima M, Funamoto S, Ihara Y (2009) γ-Secretase: successive tripeptide and tetrapeptide release from the transmembrane domain of β-carboxyl terminal fragment. J Neurosci 29: 13042-13052

Takasugi N, Tomita T, Hayashi I, Tsuruoka M, Niimura M, Takahashi Y, Thinakaran G, Iwatsubo T (2003) The role of presenilin cofactors in the γ-secretase complex. Nature 422: 438-441

Wada S, Morishima-Kawashima M, Qi Y, Misonou H, Shimada Y, Ohno-Iwashita Y, Ihara Y (2003) Gamma-secretase activity is present in rafts but is not cholesterol-dependent. Biochemistry 47: 13977-13986

Weggen S, Eriksen JL, Das P, Sagi SA, Wang R, Pietrzik CU, Findlay KA, Smith TE, Murphy MP, Bulter T, *et al* (2001) A subset of NSAIDs lower amyloidogenic Aβ42 independently of cyclooxygenase activity. Nature 414: 212-216

Winblad B, Palmer K, Kivipelto M, Jelic V, Fratiglioni L, Wahlund LO, Nordberg A, Backman L, Albert M, Almkvist O, *et al* (2004) Mild cognitive impairment—beyond controversies, towards a consensus: report of the International Working Group on Mild Cognitive Impairment. J Intern Med 256: 240-246

Yang DS, Tandon A, Chen F, Yu G, Yu H, Arakawa S, Hasegawa H, Duthie M, Schmidt SD, Ramabhadran TV, *et al* (2002) Mature glycosylation and trafficking of nicastrin modulate its binding to presenilins. J Biol Chem 277: 28135-28142

Zou K, Yamaguchi H, Akatsu H, Sakamoto T, Ko M, Mizoguchi K, Gong JS, Yu W, Yamamoto T, Kosaka K, *et al* (2007) Angiotensin-converting enzyme converts amyloid β-protein 1–42 (Aβ(1–42)) to Aβ(1–40), and its inhibition enhances brain Aβ deposition. J Neurosci 27: 8628-8635

doi:10.1093/brain/aws230 Brain 2012: 135; 3380–3391 | 3380

BRAIN
A JOURNAL OF NEUROLOGY

Molecular analysis and biochemical classification of TDP-43 proteinopathy

Hiroshi Tsuji,[1,2] Tetsuaki Arai,[3,4] Fuyuki Kametani,[1] Takashi Nonaka,[1] Makiko Yamashita,[1] Masami Suzukake,[1] Masato Hosokawa,[3] Mari Yoshida,[5] Hiroyuki Hatsuta,[6] Masaki Takao,[6] Yuko Saito,[7] Shigeo Murayama,[6] Haruhiko Akiyama,[3] Masato Hasegawa,[1] David M. A. Mann[8] and Akira Tamaoka[2]

1 Department of Neuropathology and Cell Biology, Tokyo Metropolitan Institute of Medical Science, Tokyo 156-8585, Japan
2 Department of Neurology, Graduate School of Comprehensive Human Sciences, University of Tsukuba, Tsukuba-shi 305-8576, Japan
3 Department of Dementia and Higher Brain Function, Tokyo Metropolitan Institute of Medical Science, Tokyo 156-8585, Japan
4 Department of Psychiatry, Graduate School of Comprehensive Human Sciences, University of Tsukuba, Tsukuba-shi 305-8576, Japan
5 Department of Neuropathology, Institute for Medical Science of Aging, Aichi Medical University, Aichi 480-1195, Japan
6 Department of Neuropathology, Tokyo Metropolitan Institute of Gerontology, Tokyo 173-0015, Japan
7 Department of Pathology and Laboratory Medicine, National Center Hospital of Neurology and Psychiatry, Tokyo 187-8551, Japan
8 Mental Health and Neurodegeneration Research Group, Greater Manchester Neuroscience Centre, University of Manchester, Manchester M13 9PT, UK

Correspondence to: Masato Hasegawa,
Department of Neuropathology and Cell Biology,
Tokyo Metropolitan Institute of Medical Science,
2-1-6 Kamikitazawa,
Setagaya-ku,
Tokyo 156-8506,
Japan
E-mail: hasegawa-ms@igakuken.or.jp

Amyotrophic lateral sclerosis and frontotemporal lobar degeneration with TAR DNA-binding protein of 43 kDa pathology are progressive neurodegenerative diseases that are characterized by intracytoplasmic aggregates of hyperphosphorylated TAR DNA-binding protein of 43 kDa. These TAR DNA-binding protein 43 proteinopathies can be classified into subtypes, which are closely correlated with clinicopathological phenotypes, although the differences in the molecular species of TAR DNA-binding protein 43 in these diseases and the biological significance thereof, remain to be clarified. Here, we have shown that although the banding patterns of abnormally phosphorylated C-terminal fragments of TAR DNA-binding protein 43 differ between the neuropathological subtypes, these are indistinguishable between multiple brain regions and spinal cord in individual patients. Immunoblot analysis of protease-resistant TAR DNA-binding protein 43 demonstrated that the fragment patterns represent different conformations of TAR DNA-binding protein 43 molecular species in the diseases. These results suggest a new clinicopathological classification of TAR DNA-binding protein 43 proteinopathies based on their molecular properties.

Keywords: amyotrophic lateral sclerosis; frontotemporal lobar degeneration; TDP-43; classification

Abbreviations: ALS = amyotrophic lateral sclerosis; FTLD = frontotemporal lobar degeneration; FTLD-TDP = frontotemporal lobar degeneration with TAR DNA-binding protein of 43 kDa pathology; TDP-43 = TAR DNA-binding protein of 43 kDa

Received March 13, 2012. Revised June 3, 2012. Accepted June 28, 2012. Advance Access publication October 3, 2012

Introduction

Amyotrophic lateral sclerosis (ALS) and frontotemporal lobar degeneration with TDP-43 pathology (FTLD-TDP) are sporadic and familial neurodegenerative diseases characterized neuropathologically by intracytoplasmic aggregates of TAR DNA-binding protein of 43 kDa (TDP-43) (Arai *et al.*, 2006; Neumann *et al.*, 2006). In ALS, upper and lower motor neurons progressively degenerate. Neuropathologically, the TDP-43-positive structures appear as rounded or skein-like inclusions in the lower motor neurons. Similar TDP-43-positive inclusions are also observed in the prefrontal gyrus that contains the upper motor neurons. Moreover, TDP-43-positive glial cytoplasmic inclusions are found close to the upper and lower motor neurons in ALS (Tan *et al.*, 2007). In FTLD-TDP, TDP-43 pathology is distinguished into four histological subtypes (types A–D) based on the predominant type of TDP-43-positive structures present (Mackenzie *et al.*, 2011). Type A is characterized by numerous short dystrophic neurites and crescentic or oval neuronal cytoplasmic inclusions; type B has moderate numbers of neuronal cytoplasmic inclusions, throughout all cortical layers, but few dystrophic neurites; type C has a predominance of elongated dystrophic neurites in upper cortical layers, with few neuronal cytoplasmic inclusions; and type D refers to the pathology associated with inclusion body myopathy with early onset Paget disease and frontotemporal dementia caused by *VCP* mutations, characterized by numerous short dystrophic neurites and frequent lentiform neuronal intranuclear inclusions. There is a relationship between subtypes of TDP-43 pathology and clinical phenotype, and many cases of ALS and frontotemporal lobar degeneration (FTLD) are readily distinguished by each clinical symptom. However, some cases have symptoms of both ALS and FTLD. ALS with dementia refers to cases initially presenting with motor neuron disease becoming demented, whereas FTLD-motor neuron disease refers to cases presenting with cognitive impairment and subsequently developing motor neuron disease.

TDP-43 pathology is also present in a subset of familial ALS and FTLD due to mutations in *TARDBP* (Kabashi *et al.*, 2008; Sreedharan *et al.*, 2008), progranulin (*GRN*; Baker *et al.*, 2006) and *C9ORF72* (DeJesus-Hernandez *et al.*, 2011; Renton *et al.*, 2011) genes. Although most patients with mutations in *TARDBP* present with ALS, some present with FTLD (Gitcho *et al.*, 2009; Kovacs *et al.*, 2009). Cases with FTLD-TDP with *GRN* mutation often show type A pathology (Mackenzie *et al.*, 2006b; Cairns *et al.*, 2007b; Josephs *et al.*, 2007). The pathology of ALS and FTLD due to mutations in *C9ORF72* is heterogeneous: TDP-43 pathology overlaps between ALS and FTLD-TDP types A and B (Murray *et al.*, 2011). One large multicentre study of sporadic and familial FTLD-TDP showed broad overlap between the TDP-43 subtyping, especially between types A and B (Armstrong *et al.*, 2010). These overlaps might occur because current pathological classification may be inadequate, as it is based solely on the morphological assessment of certain subjective cortical regions. A more objective and unbiased classification is needed.

In this study, we have investigated a wide range of patients with various TDP-43 proteinopathies to investigate whether patterns of protease-resistant TDP-43 might indicate different TDP-43 strain types, and characterize the TDP-43 C-terminal banding patterns in multiple regions of the CNS, basing our approach on the method used for demonstration of prion strain variation and the aetiology of new variant Creutzfeldt–Jakob disease (Collinge *et al.*, 1996). We show at least three C-terminal banding patterns that distinguish diseases with TDP-43 proteinopathy and report that the banding pattern in individual patients is indistinguishable in different brain regions and spinal cord. Corresponding patterns of protease-resistant phosphorylated TDP-43 are also seen between the pathological phenotypes. As with the prion diseases, the present results suggest that the different conformation of abnormal TDP-43 deposits in the CNS in patients corresponding with various subtypes of TDP-43 proteinopathy, and that the conformation state of the abnormal TDP-43 protein may determine the pathological phenotype.

Materials and methods

Patients

Human brain tissues were obtained from the Brain Donation Programme at the University of Tsukuba (Japan), Tokyo Metropolitan Institute of Gerontology (Japan), National Shimofusa Mental Hospital (Japan) and the University of Manchester (UK). This study was approved by the local Research Ethics Committee. The subjects in this study included eight patients with ALS, five patients with FTLD-TDP type A, eight patients with FTLD-TDP type B, six patients with FTLD-TDP type C and two patients with Alzheimer's disease without TDP-43 pathology. All cases with ALS met the revised El Escorial criteria for ALS (Brooks, 1994) without dementia. All cases with FTLD-TDP fulfilled clinical diagnostic criteria of FTLD (Neary *et al.*, 1998), and classifications of TDP-43 subtype were made in accordance with published guidelines (Cairns *et al.*, 2007a; Mackenzie *et al.*, 2011). Four patients with FTLD-TDP type A were cases of familial FTLD-U with *GRN* mutations. One familial ALS case, one with type A, and two with type B had the GGGCC repeat expansion in *C9ORF72*. The age, gender, brain regions examined and clinical diagnosis are given in Table 1.

A fresh frozen tissue sample was taken and cut into two pieces. One piece was fixed in 4% paraformaldehyde in 0.1 M phosphate buffer (pH 7.4) for 2 days and was used for immunohistochemical analysis. The other piece was homogenized and used for immunoblot analysis. In principle, we took the precentral gyrus and lumbar part of the spinal cord in the ALS cases, and the frontal lobe in the FTLD-TDP cases, because TDP-43 pathology is always known to be prevalent in these regions (Tan *et al.*, 2007; Geser *et al.*, 2008, 2009). However, the spinal cord was not available in four cases with ALS, and both motor regions in two cases were not available. In these cases, the frontal lobe was examined instead. For ALS Cases 1, 3, 5 and ALS and FTLD-TDP type C Case 22, the whole of the cerebral hemisphere and brainstem were available as fresh frozen tissues. In these four cases, we took the multiple regions, as described in Table 1. Every tissue sample was examined immunohistochemically for TDP-43-positive lesions. All samples, except some from the cerebellar cortex, showed an accumulation of abnormal TDP-43-positive structures.

Immunoblotting

Sarkosyl-insoluble, urea-soluble fractions were extracted from each region as previously described (Arai *et al.*, 2006; Hasegawa *et al.*, 2008).

Table 1 **Description of the patients**

Case number	Age at death (year)	Age at onset (year)	Sex	Family history	Brain weight (g)	Clinical diagnosis	Region
ALS							
1	62	61	M	N	1150	ALS	Prec, L and other regions[a]
2	72	71	F	N	1390	ALS	Prec and L
3	42	40	F	N	1140	ALS	Prec, L and other regions[a]
4	76	75	F	N	NA	ALS	Prec and L
5	62	54	M	N	1230	ALS	Prec and other regions[a]
6	77	76	F	N	NA	ALS	Prec
7	67	65	M	N	1414	ALS	Fr
8	55	53	M	Y(m*C9ORF72*)	1250	ALS	Fr
FTLD-TDP type A							
9	58	49	M	Y(m*C9ORF72*)	1050	FTD	Fr
10	67	54	F	Y(m*GRN*)	NA	FTD	Fr
11	71	63	F	Y(m*GRN*)	863	PNFA	Fr
12	66	56	F	Y(m*GRN*)	1100	FTD	Fr
13	68	60	M	Y(m*GRN*)	1210	FTD + MND	Fr
FTLD-TDP type B							
14	45	43	M	N	1260	FTD + MND	Fr
15	59	57	M	Y(m*C9ORF72*)	1210	FTD + MND	Fr
16	67	65	M	N	1280	FTD + MND	Fr
17	76	74	M	N	1215	FTD + MND	Fr
18	69	58	M	N	1166	FTD + MND	Fr
19	52	50	F	Y(m*C9ORF72*)	1050	FTD + MND	Fr
20	65	61	M	N	1530	FTD + MND	Fr
21	68	64	M	N	1213	FTD + MND	Fr
FTLD-TDP type C							
22	82	NA	M	N	1200	SD	Fr, Te and other regions[b]
23	67	65	M	N	NA	SD	Fr
24	59	53	M	N	NA	SD	Fr
25	63	58	M	N	NA	SD	Fr
26	66	55	F	N	1035	SD	Fr
27	75	60	M	N	1174	SD	Fr
AD							
28	65	56	F	N	1165	AD	Fr
29	70	NA	F	N	1126	AD	Fr

AD = Alzheimer's disease; Fr = frontal cortex; FTD = frontotemporal dementia; L = lumbar part of spinal cord; m*C9ORF72* = mutation of chromosome 9 open-reading frame 72 gene; m*GRN* = mutation of progranulin gene; MND = motor neuron disease; NA = not available; PNFA = progressive non-fluent aphasia; Prec = precentral gyrus; SD = semantic dementia; Y = yes; N = no.

a Other regions contained striatum, thalamus, hippocampus dentate gyrus, substantia nigra, pons, medulla and cerebellum cortex. In these cases, the grey and white matter of precentral gyrus were separated from each other macroscopically and examined.

b Other regions contain striatum, thalamus, hippocampus dentate gyrus, substantia nigra, pons, medulla and cerebellum cortex. FTLD-TDP type B without MND and type D are not analysed in this study.

The samples were loaded on 15% SDS–PAGE gels. Proteins in the gel were then transferred onto a polyvinylidene difluoride membrane (Millipore). After blocking with 3% gelatine in 0.01 M PBS (pH 7.4), membranes were incubated overnight with phosphorylation dependent anti-TDP-43 rabbit polyclonal antibody (pS409/410, 1:1000; Hasegawa *et al.*, 2008), phosphorylation independent TDP-43 polyclonal antibody 10782-1-AP (TDP-43 pAb, 1:3000) and TDP-43 monoclonal antibody, 60019-2-Ig (TDP-43 mAb, 1:3000) (ProteinTech Group). After incubation with the appropriate biotinylated secondary antibody, immunolabelling was detected using the VECTASTAIN® ABC system (Vector Laboratories) coupled with a 3,3′-diaminobenzidine reaction intensified with nickel chloride. The blot membranes were digitally analysed, and densitometric analyses were performed with ImageJ version 1.44p (NIH, http://rsbweb.nih.gov/ij/index.html). The densitometry data were averaged for all cases in each group to illustrate the different patterns.

Immunohistochemistry

After cryoprotection in 15% sucrose in 0.01 M PBS (pH 7.4), paraformaldehyde-fixed tissue blocks were cut on a freezing microtome at 30-μm thickness. The free-floating sections were immunostained with phosphorylation-dependent TDP-43 monoclonal antibody (pS409/410, 1:10 000) (Inukai *et al.*, 2008) for 72 h in the cold. After treatment with mouse secondary antibody, immunolabelling was detected using the VECTASTAIN ®ABC system coupled with a 3,3′-diaminobenzidine reaction to yield a brown precipitate. Sections were lightly counterstained with heamatoxylin.

Protease treatment of phosphorylated TDP-43

Sarkosyl-insoluble fractions extracted from the neocortical regions of patients with ALS or FTLD-TDP were treated with final concentration of 100 μg/ml trypsin (Promega) or 10 μg/ml chymotrypsin (Sigma-Aldrich) at 37°C for 30 min. The reaction was stopped by boiling for 5 min. After centrifuging at 15 000 rpm for 1 min, the samples were analysed by immunoblotting as described earlier.

Mass spectrometry

Sarkosyl-insoluble, trypsin-resistant fractions were loaded on 15% SDS–PAGE gels. The pS409/410-positive ~16 kDa bands were dissected and digested in-gel with chymotrypsin. The digests were applied to the Paradigm MS4 high-performance liquid chromatography system (Microm BioResources). A reversed phase capillary column (Develosil ODS-HG5, 0.075 × 150 mm, Nomura Chemical) was used at a flow rate of 300 nl/min with a 4–80% linear gradient of acetonitrile in 0.1% formic acid. Eluted peptides were directly detected with an ion trap mass spectrometer, LXQ (Thermo Fisher Scientific). The obtained spectra were analysed with Mascot (Matrix Science).

Statistical analysis

The *P*-values for the description of the statistical significance of differences were calculated by means of the paired, two-tailed *t*-test using Prism 5.04 software (GraphPad Software, Inc).

Results

Banding patterns of phosphorylated C-terminal TDP-43 in ALS and FTLD with TDP-43 pathology

Immunoblot analysis using an antibody specific for abnormal TDP-43, pS409/410, showed high-molecular-weight smearing substances, phosphorylated full-length TDP-43 at 45 kDa and several C-terminal fragments at 18–26 kDa to be present in affected brain regions in all cases (Fig. 1). Three major bands at 23, 24 and 26 kDa, and two minor bands at 18 and 19 kDa were seen in the precentral gyrus and frontal cortex of cases with ALS, with the 24 kDa band being the most intense (Fig. 1A and F). In the lumbar spinal cord, the two minor bands at 18 and 19 kDa were barely present, but the banding pattern of the three major bands at 23, 24 and 26 kDa was similar to that in the cerebral cortex (Fig. 1A). No such pS409/410-positive TDP-43 bands were detected in control cases with Alzheimer's disease with no TDP-43 pathology (Fig. 1B). In the FTLD-TDP cases, the banding pattern could be distinguished into three types according to the FTLD-TDP histological subtype (Fig. 1C–E). In FTLD-TDP type A, three major bands at 23, 24 and 26 kDa, and two minor bands at 18 and 19 kDa were detected, with the 23 kDa band being the most intense (Fig. 1C and F). In FTLD-type B cases, the banding pattern was the same as that in the ALS cases (Fig. 1D and F). In FTLD-TDP type C cases, two major bands at 23 and 24 kDa, and two minor bands at 18 and 19 kDa were detected, with the 24 kDa band being the most intense, and the band at 26 kDa being hardly detectable (Fig. 1E and F). Densitometric analyses of the immunoblots for all cases are shown in Supplementary Fig. 1. Each component of the C-terminal fragments was significantly different (Fig. 1F).

Immunoblot analysis using phosphorylation independent TDP-43 polyclonal and monoclonal antibodies detected phosphorylated full-length TDP-43 at 45 kDa, two bands ~25 kDa and high-molecular-weight smears, in addition to the normal TDP-43 band at 43 kDa in ALS and various subtypes of FTLD-TDP. The banding patterns between ALS and various subtypes of FTLD-TDP could not be distinguished with these antibodies. In the cases with Alzheimer's disease, the normal TDP-43 band at 43 kDa was detected, but neither the phosphorylated 45 kDa band nor the ~25 kDa fragments were observed (Supplementary Fig. 2). Immunoblot analysis of α-tubulin in Tris saline-soluble fractions from cases with types A, B and C pathology showed no correlation between the banding pattern of α-tubulin and that of TDP-43 (Supplementary Fig. 3), indicating that the differences in the banding patterns are not because of protein degradation caused by a long post-mortem interval or unfavourable agonal status.

Immunohistochemistry and immunoblot analyses of phosphorylated TDP-43 in multiple regions of ALS and FTLD with TDP-43 pathology

In ALS cases, the neuronal cytoplasmic pathology, which included skein-like inclusions, irregularly shaped TDP-immunoreactive neuronal cytoplasmic inclusions and densely staining granules, was confirmed in multiple regions by immunohistochemistry analysis using pS409/410 (Fig. 2A–G). Glial cytoplasmic inclusions were also present in many regions. Glial cytoplasmic inclusions were more frequent in the white matter than in the grey matter (Fig. 2H). A few neuronal cytoplasmic inclusions were found in the cerebellar cortex granule cells (Fig. 2G). In FTLD-TDP type C, dystrophic neurites were seen in multiple regions except for the cerebellar cortex (Fig. 2I–O), whereas neuronal cytoplasmic inclusions were also present in the striatum and hippocampus dentate gyrus granule cells (Fig. 2J and L). No abnormal structures were found in the cerebellar cortex (data not shown). These observations show that pathological TDP-43 is present throughout many CNS areas in ALS, suggesting that ALS does not selectively affect only the motor system, but it is rather a multisystem neurodegenerative TDP-43 proteinopathy.

Immunoblot analyses of three ALS cases confirmed that phosphorylated TDP-43 and the C-terminal fragments are deposited in multiple brain regions in ALS (Fig. 3A). Relatively strong immunoreactivities were detected in the striatum (in Cases 3 and 5) and substantia nigra (in Cases 1 and 5), although this varied between cases (Fig. 3A). Importantly, the banding pattern for the TDP-43 C-terminal fragments in these three cases was basically the same in all brain regions examined (Fig. 3A). In FTLD-TDP type C, a C-terminal banding pattern, clearly distinct from that

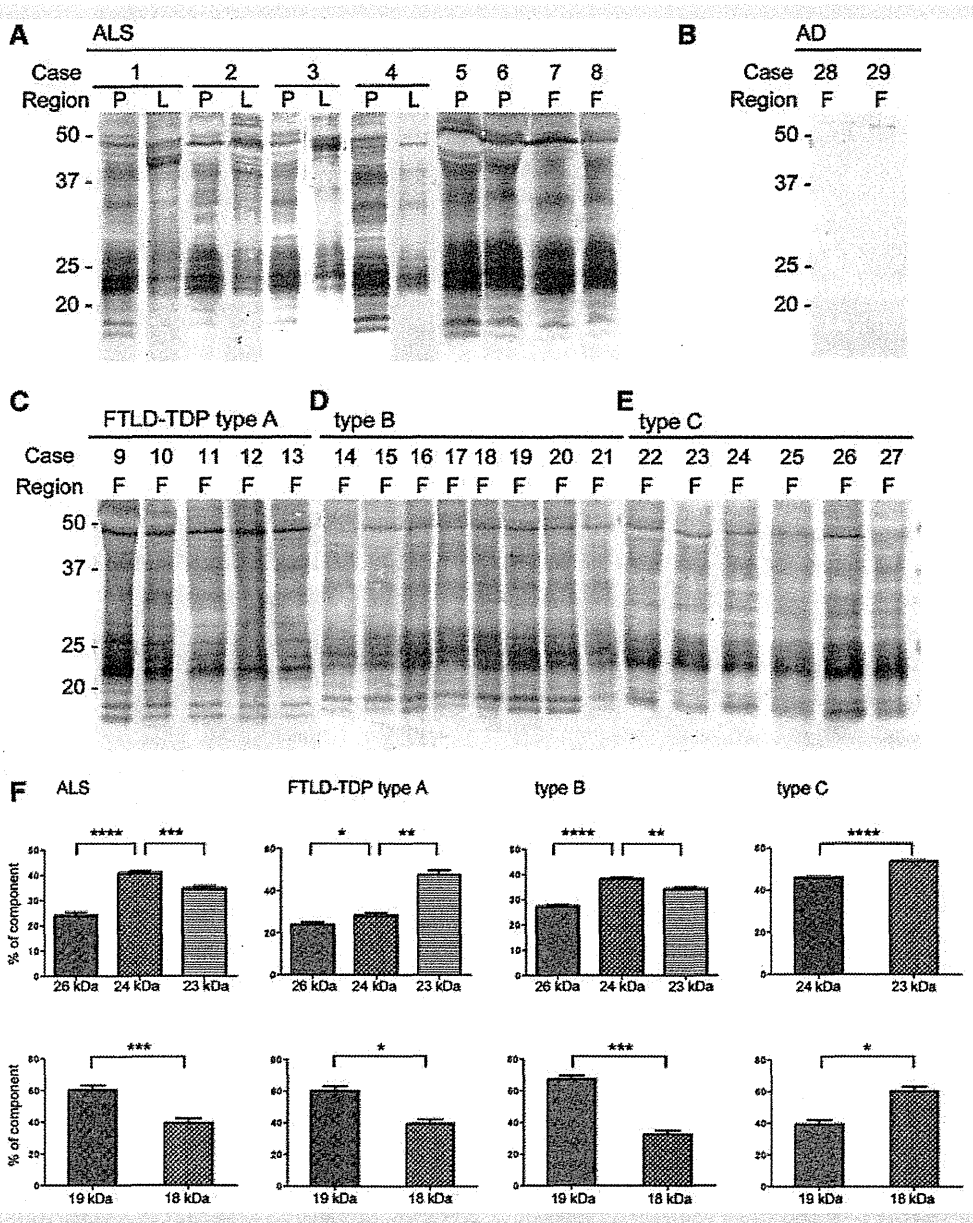

Figure 1 Immunoblot analyses of sarkosyl-insoluble TDP-43 in the brains or spinal cords of ALS (Cases 1–8) (**A**), Alzheimer's disease (Cases 28–29) (**B**), FTLD-TDP type A (Cases 9–13) (**C**), FTLD-TDP type B (Cases 14–21) (**D**) and FTLD-TDP type C (Cases 22–27) (**E**), using a phosphorylation-dependent anti-TDP-43 antibody (pS409/410). In all cases, high-molecular-weight smearing substances, phosphorylated full-length TDP-43 at 45 kDa and several C-terminal fragments at 18–26 kDa are detected. In ALS (**A**) and FTLD-TDP type B (**D**) cases, three major bands at 23, 24 and 26 kDa and two minor bands at 18 and 19 kDa are detected, whereas in the FTLD-TDP Type C (**E**) cases, two major bands at 23 and 24 and two minor bands at 18 and 19 kDa. A 24 kDa band is the most intense in ALS (**A**) and FTLD-TDP type B (**E**), whereas a 23 kDa band is the most intense in FTLD-TDP type C (**D**). The band pattern of the cases with type A (**C**) is an intermediate between FTLD-TDP type B (**D**) and FTLD-TDP type C (**E**). In spinal cords of cases with ALS, the 18 and 19 kDa bands are hardly detectable, but the same banding pattern of the 23–26 kDa bands as in precentral gyrus is detected. No such TDP-43 fragments are detected in brains of patients with Alzheimer's disease (AD) (**B**). The intensity of each C-terminal band was analysed using the ImageJ software and each component was statistically analysed by Student's *t*-test (**F**). Data indicate mean (SEM). $^{****}P < 0.0001$, $^{***}P < 0.001$, $^{**}P < 0.01$, $^{*}P < 0.05$. F = frontal cortex; L = lumbar part of spinal cord; P = precentral cortex.

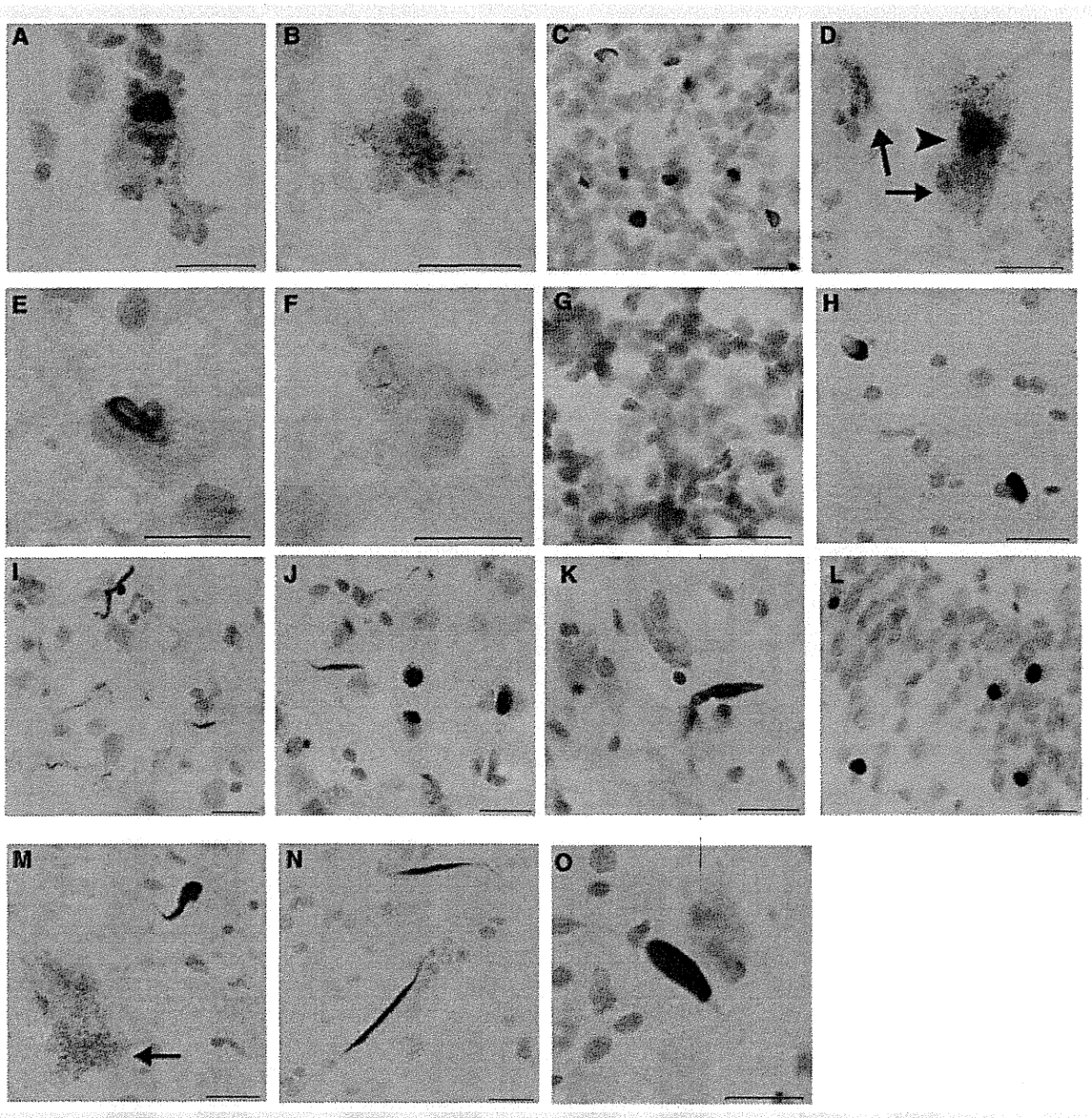

Figure 2 Phosphorylated TDP-43-positive structures observed in different brain regions and spinal cords of ALS (**A–H**) and FTLD-type C (**I–O**) using a phosphorylation-dependent anti-TDP-43 antibody (pS409/410). (**A**) Lewy body-like inclusion in the striatum neuron. (**B**) Cytoplasmic granular staining in the thalamus. (**C**) Neuronal cytoplasmic inclusions in the granular cells of hippocampus. (**D**) Irregularly shaped TDP-immunoreactive neuronal cytoplasmic inclusion in the substantia nigra (arrowhead). The arrows denote neuromelanin granules. (**E**) Skein-like inclusion in the motor nucleus of trigeminal nerve of pons. (**F**) Skein-like inclusion in the inferior olivary nucleus of medulla. (**G**) Neuronal cytoplasmic inclusion in the granular cells of cerebellar cortex. (**H**) Glial cytoplasmic inclusions in the white matter of precentral cortex. (**I**) Dystrophic neurites in the temporal cortex, (**J**) dystrophic neurites and neuronal cytoplasmic inclusions in the striatum. (**K**) Dystrophic neurites in the thalamus. (**L**) Neuronal cytoplasmic inclusions in the granular cells of hippocampus. (**M**) Dystrophic neurites in the substantia nigra. The arrow denotes neuromelanin granules. (**N**) Dystrophic neurites in the pons. (**O**) Dystrophic neurites in the medullary reticular formation. Scale bars = 20 μm.

of ALS, was detected in the temporal cortex, striatum and hippocampus, but was barely detected in the thalamus, substantia nigra, pons and medulla, and not at all in the cerebellar cortex (Fig. 3B). The banding pattern observed in these brain regions was indistinguishable (Fig. 3B). These results suggest that the same abnormal TDP-43 molecular species is deposited in different brain regions and different cell types, although the morphology of the TDP-43 inclusions may be different in the brain regions. Densitometric analyses of the immunoblots for all cases are shown in Supplementary Fig. 4.

Protease-resistant TDP-43 in ALS and FTLD with frontotemporal dementia-43 pathology

These different banding patterns in TDP-43 proteinopathies may represent different conformations of abnormal TDP-43 or their aggregates. To test this hypothesis, we subjected the abnormal TDP-43 recovered in the sarkosyl-insoluble pellets to protease treatment and analysed the protease-resistant bands. Proteins can be easily cleaved by proteases if they are denatured or unstructured, but domains that have rigid structures, such as a β-sheet conformation or that are structurally buried or interacting with other molecules, are highly resistant to proteases. On trypsin or chymotrypsin treatment, the full-length 45-kDa band and the smearing substance of TDP-43 disappeared, leaving protease-resistant fragments at 16–25 kDa (Figs 4 and 5). As expected, the protease-resistant banding patterns were different and distinguishable into three patterns (Figs 4 and 5). In ALS, trypsin-resistant doublet bands at 16 and 15 kDa, and two minor bands at ~24 kDa were detected, whereas a single band at 16 kDa and some additional bands at ~24 kDa were detected in FTLD-TDP type A (Fig. 4A, Lanes 1 and 2). In FTLD-TDP type B, the same banding pattern as that in ALS was observed (Fig. 4A, Lane 3). In FTLD-TDP type C, a broad single band at 16 kDa and some additional bands at ~24 kDa were detected (Fig. 4A, Lane 4). No such bands were detected in Alzheimer's disease (Fig. 4A, Lane 5).

Similarly, on chymotrypsin treatment, multiple protease-resistant bands were detected at 16–25 kDa and the chymotrypsin-resistant band patterns were also different between the three disease subtypes (Fig. 4B). Doublet bands were seen in ALS and FTLD-TDP type B, but only a single band in FTLD-TDP type C was detected at ~16 kDa (Fig. 4B). In FTLD-TDP type A, the lower band (15 kDa) of the ~16 kDa doublet was more intense than the upper one (16 kDa).

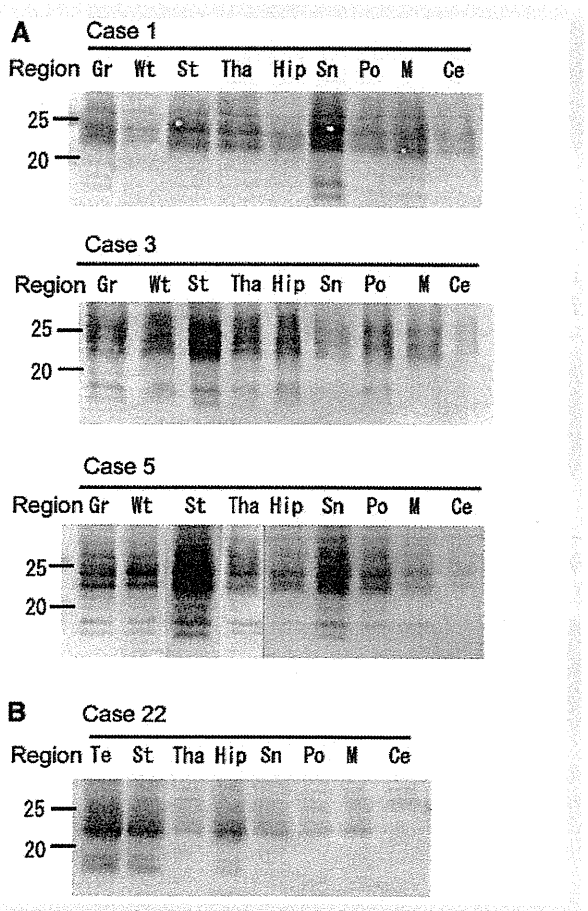

Figure 3 Immunoblot analyses of the C-terminal fragments of phosphorylated TDP-43 in the different brain regions of cases with ALS (Cases 1, 3 and 5, as shown in Fig. 1) **(A)** and FTLD-type C (Case 22, as shown in Fig. 1) **(B)**. **(A)** Immunoblots of insoluble TDP-43 in the grey or white matter of precentral cortex, striatum, thalamus, hippocampus, substantia nigra, pons and medulla of ALS cases. **(B)** Immunoblot of TDP-43 in temporal cortex, striatum, hippocampus, thalamus, substantia nigra, pons and cerebellar cortex of the case with FTLD-TDP type C. Ce = Cerebellar cortex; Gr = grey matter of precentral gyrus; Hip = hippocampus; M = medulla; Po = pons; Sn = substantia nigra; St = striatum; Tha = thalamus; Te = temporal cortex; Wt = white matter of precentral gyrus. Immunoblots of spinal cords of cases with ALS are shown in Fig. 1.

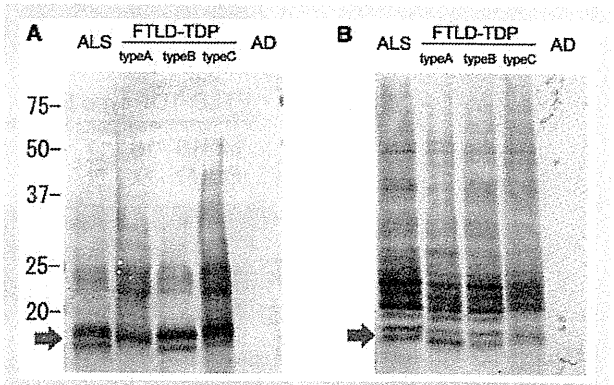

Figure 4 Immunoblot analysis of phosphorylated TDP-43 from representative ALS and FTLD-TDP cases after protease treatment. **(A)** Immunoblot of insoluble TDP-43 from cases with ALS, FTLD-TDP type A, type B, type C and Alzheimer's disease (AD) after trypsin treatment. Doublet bands at ~16 kDa (arrow) and some minor 23–24 kDa bands are detected in ALS and FTLD-TDP type B, whereas a single band at ~16 kDa and several bands at 23 and 24 kDa are detected in FTLD-TDP type A and type C. No such bands are detected in the Alzheimer's disease case. **(B)** Immunoblot of insoluble TDP-43 from cases with ALS, FTLD-TDP type A, type B, type C and Alzheimer's disease after chymotrypsin treatment. Multiple protease-resistant TDP-43 bands are detected at 16–25 kDa. Doublet bands at ~16 kD (arrow) are detected in ALS and FTLD-TDP type A and B, whereas a single band at ~16 kD (arrow) is detected in the case with FTLD-TDP type C. In FTLD-TDP type A, the lower band of the doublet at 16 kDa is more intense. No such bands are detected in the Alzheimer's disease case.

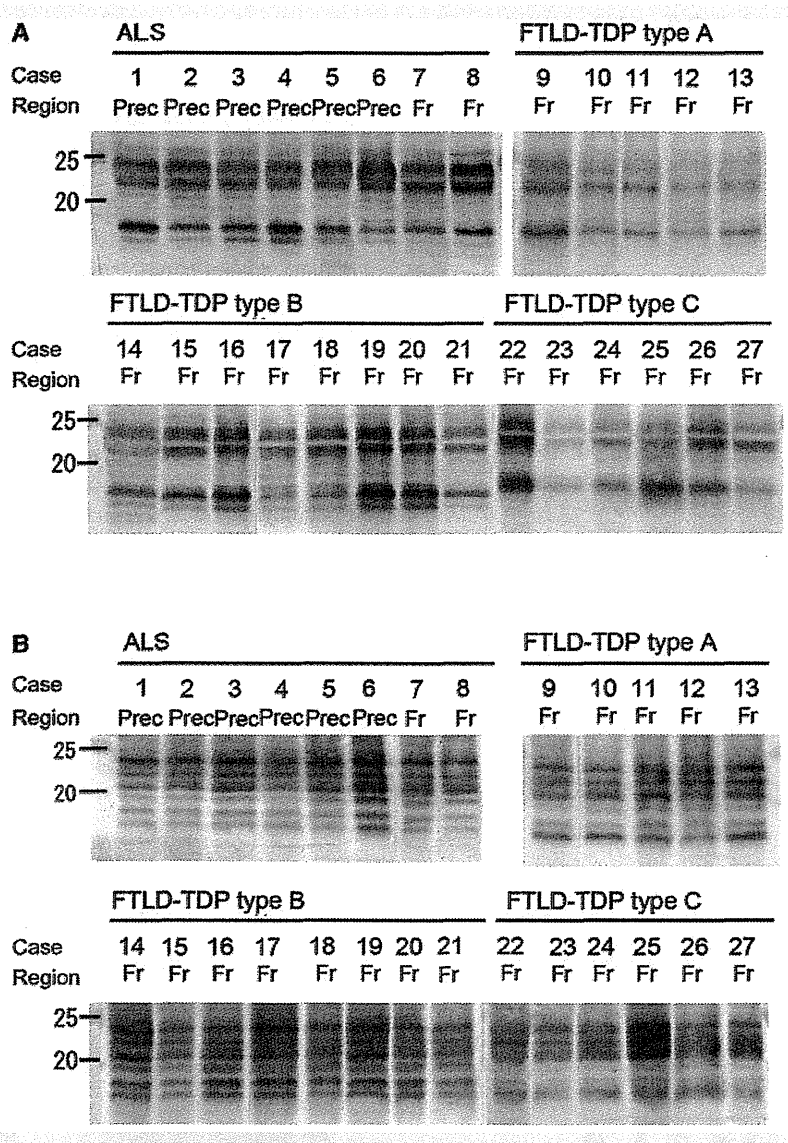

Figure 5 Comparison of the protease-resistant TDP-43 banding patterns in ALS and FTLD-TDP. Immunoblot analyses of trypsin-resistant (**A**) and chymotrypsin-resistant (**B**) fragments of TDP-43 from all cases examined. The banding patterns of ALS and FTLD-TDP type B cases are indistinguishable. Fr = frontal cortex; Prec = precentral gyrus.

In all cases examined, the trypsin-resistant banding patterns were clearly distinguishable between the disease subtypes in accordance with the three different types of banding pattern of TDP-43 C-terminal fragments, although it is difficult to distinguish the trypsin band pattern of type A from that of type C (Figs 5A, 6A and Supplementary Fig. 5). The chymotrypsin-resistant banding patterns were distinguishable and could be differentiated into three types (Figs 5B, 6B and Supplementary Fig. 6), also in accordance with the banding pattern of the TDP-43 C-terminal fragment. The banding patterns of ALS and FTLD-TDP type B were the same, whereas the banding pattern of FTLD-TDP type A was distinguishable from those of type C and type B (Figs 4 and 5). The combination analyses of trypsin and chymotrypsin-resistant banding patterns confirmed that TDP-43 proteinopathies can also be biochemically distinguishable into three types according to TDP-43 subtypes. These results strongly suggest that the different C-terminal banding patterns represent different conformations of TDP-43 aggregates and that the distinct types of TDP-43 are deposited in association with distinct pathological phenotypes of TDP-43 proteinopathies.

Immunoblot analysis using phosphorylation independent TDP-43 polyclonal and monoclonal antibodies detected some TDP-43 fragments in the ALS and FTLD-TDP cases after trypsin or chymotrypsin treatment, although no clear difference was observed in the banding patterns between ALS and other subtypes of FTLD-TDP (Supplementary Fig. 7). The distinctive

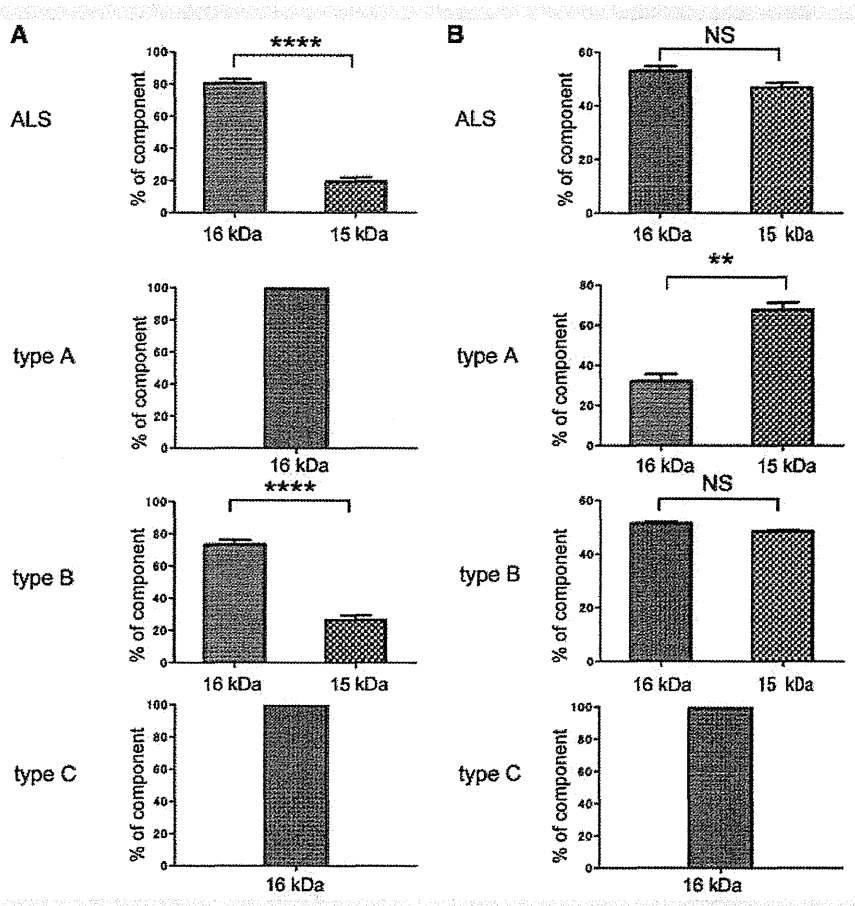

Figure 6 Quantitative analysis of protease-resistant ~16 kDa band. **(A)** The intensity of trypsin-resistant ~16 kDa band of each case was quantitated with ImageJ and statistically analysed. **(B)** The intensity of chymotrypsin-resistant ~16 kDa band of each case was quantitated with ImageJ and statistically analysed. Data indicate mean (SEM). $****P < 0.0001$, $**P < 0.01$, NS = not significant.

protease-resistant bands at ~16 kDa of ALS were not detected with both phosphorylation independent antibodies (Supplementary Fig. 8).

We also analysed the banding pattern of phosphorylated TDP-43 in another series of five sporadic cases with TDP-43 pathology (Alzheimer's disease, Alzheimer's disease/dementia with Lewy bodies and Alzheimer's disease/argyrophilic grain disease) (Supplementary Table 1). The banding pattern of the C-terminal fragments, and trypsin- or chymotrypsin-resistant fragments, in these were same as those of FTLD-TDP type A with *GRN* mutation (Supplementary Fig. 9).

Mass spectrometric analysis of protease-resistant bands of TDP-43 in ALS and FTLD-TDP type C

To further investigate the differences in the abnormal TDP-43 protein species at a molecular level, we analysed the ~16 kDa trypsin-resistant bands by mass spectrometry. Mass analysis of chymotrypsin digests of ~16 kDa trypsin-resistant fragments identified 4 peptides, amino acid residues 277–289, 290–299, 294–333 and 300–316, suggesting these peptides are derived from trypsin-resistant fragments 276–414 and 294–414. Mass spectrometric analysis of the single broad band from FTLD-TDP type C identified the peptides of amino acids 273–283, 277–289, 290–313 and 317–330, strongly suggesting that the trypsin-resistant fragments from FTLD-TDP type C are derived from peptides 273–414 and 276–414. These analyses clearly indicate that trypsin-resistant core regions of the abnormal TDP-43 accumulated in the brain are not necessarily the same between ALS and FTLD (Supplementary Fig. 10).

Discussion

In this study, we have shown that the banding patterns for TDP-43 C-terminal fragments in ALS and FTLD are distinguishable and classifiable into at least three types. This difference was consistently demonstrated in 27 cases, eight with ALS, five with FTLD-TDP type A, eight with FTLD-TDP type B and six with FTLD-TDP type C. These results strongly suggest that distinct

types of TDP-43 molecules constitute the distinct types of pathologies of TDP-43 and determine the clinicopathological phenotypes of TDP-43 proteinopathies. In TDP-43 histopathology, ALS is considered to represent a distinct pathological subtype because the distribution of TDP-43 inclusions is different from that of FTLD-TDP (Mackenzie *et al.*, 2006a). However, as shown in this study, the TDP-43 accumulations in ALS and FTLD-TDP type B are biochemically indistinguishable. In fact, clinical and histopathological motor neuron disease is often present in cases with FTLD-TDP type B histology. In the three types of phosphorylated C-terminal TDP-43 banding pattern, the pattern seen in FTLD-TDP type C is the most distinctive, lacking the 26 kDa band detected in ALS, FTLD-TDP type A and type B cases (Fig. 1). The clinical diagnosis of the FTLD-TDP type C cases was semantic dementia in every instance, consistent with other studies showing this type of histology to be associated with semantic dementia (Mackenzie *et al.*, 2006a). FTLD is clinically classified into frontotemporal dementia, demantic dementia and progressive non-fluent aphasia, based on topographical distributions of degeneration (Neary *et al.*, 1998). In frontotemporal dementia, the bilateral frontal and temporal lobes are affected, whereas the bilateral temporal lobes are affected in semantic dementia and the left hemisphere in progressive non-fluent aphasia. Present data showing the most distinctive pattern of abnormal TDP-43 in type C indicate that semantic dementia may be biochemically different from frontotemporal dementia. Similar differences in tau fragment banding patterns have been shown between progressive supranuclear palsy and corticobasal degeneration (Arai *et al.*, 2004). Progressive supranuclear palsy and corticobasal degeneration are neurodegenerative diseases that are characterized by intracytoplasmic aggregates of hyperphosphorylated tau with four microtubule-binding repeats, with distinctive pathological features. Immunoblot analysis of Sarkosyl-insoluble tau demonstrated that a 33 kDa C-terminal fragment of tau band predominated in progressive supranuclear palsy, whereas two closely related bands of ~37 kDa predominated in corticobasal degeneration. The clinicopathological subtypes of these diseases may be explained by different conformations of protein aggregates or species of abnormal proteins.

Unfortunately, we were unable to obtain brain tissue samples from patients with FTLD-TDP type D (associated with *VCP* mutation; Cairns *et al.*, 2007b; Neumann *et al.*, 2007). However, because the deposition of abnormal TDP-43 in this disorder is mostly within neuronal nuclei, it is possible that the conformation of abnormal TDP-43 in FTLD-TDP type D may also differ from that in FTLD-TDP types A–C. Familial ALS and FTLD-TDP cases in which known mutations [*GRN* (Baker *et al.*, 2006) or *C9ORF72* (DeJesus-Hernandez *et al.*, 2011; Renton *et al.*, 2011)] were examined in this study. In FTLD-TDP due to *GRN* mutations, type A pathology is exclusively seen (Mackenzie *et al.*, 2006b; Cairns *et al.*, 2007b; Josephs *et al.*, 2007). All our cases with FTLD with *GRN* mutation showed the same C-terminal banding patterns of phosphorylated TDP-43 corresponding to type A histology. Some recent studies describing the clinical and pathological features of cases of FTLD-TDP with hexanucleotide repeat expansions in *C9ORF72* reported that many of the 'pure' frontotemporal dementia cases had type A pathology, whereas many of the combined frontotemporal dementia and motor neuron disease cases had type B pathology (Murray *et al.*, 2011; Boeve *et al.*, 2012; Hsiung *et al.*, 2012; Mahoney *et al.*, 2012; Simon-Sanchez *et al.*, 2012; Snowden *et al.*, 2012). Present cases with *C9ORF72* expansions included one case of ALS, one case of pure frontotemporal dementia with type A pathology, and two cases of frontotemporal dementia with motor neuron disease and type B pathology. The C-terminal banding pattern of these cases with familial ALS and frontotemporal dementia with motor neuron disease was not different from that in the sporadic ALS and FTLD-TDP type B cases, and that of the frontotemporal dementia case was not different from that in the cases with *GRN* mutation. Therefore, expansions in *C9ORF72* do not seem to influence the various types of TDP-43 C-terminal banding pattern or histological type of TDP-43 pathology.

Immunohistochemical studies using TDP-43 antibodies have shown that pathological TDP-43 is present throughout many CNS areas in ALS, suggesting that ALS does not selectively affect only the motor system, but is rather a multisystem neurodegenerative TDP-43 proteinopathy (Geser *et al.*, 2008). We also confirmed this viewpoint, immunohistochemically and biochemically, finding the same disease characteristic C-terminal fragment (banding) patterns of phosphorylated TDP-43 within the cerebral cortex, spinal cord and the other different brain regions in ALS. Although the types of pathological structures or their morphologies detected on immunohistochemistry analysis appeared different, the banding patterns for the C-terminal fragments were the same in all regions examined in three patients with ALS. This was also true for the one case with FTLD-TDP type C, where the same banding pattern of the C-terminal fragments was detected in several different brain regions beyond the frontal cortex (Fig. 3). These results strongly suggest that the same abnormal TDP-43 molecule is deposited in different brain regions in ALS (and probably also in FTLD-TDP type B) and FTLD-TDP type C, although we need to examine whether this is also true for cases with FTLD-TDP type A. Importantly, the extent of the abnormal protein pathology is closely correlated with the disease progression, such as Alzheimer's disease in tauopathies (Braak and Braak, 1991), and Parkinson's disease in α-synucleinopathies (Braak *et al.*, 2003; Saito *et al.*, 2003). However, the molecular mechanisms governing different clinicopathological phenotypes of these neurodegenerative diseases and their progression are poorly understood. Recent studies using cellular or animal models have suggested that aggregation-prone proteins, such as tau and α-synuclein, can spread to other cells and brain regions like prion disorders (Clavaguera *et al.*, 2009; Frost *et al.*, 2009; Nonaka *et al.*, 2010). The spreading of α-synuclein lesions to the grafts is also observed in Parkinson's disease brains after transplantation (Li *et al.*, 2008). However, it remains to be clarified whether the 'propagating' abnormal protein species represents a distinct 'strain type' that can be differentiated by molecular criteria in human patients or whether the species are the same in different brain regions.

We have also shown that the banding patterns of protease-resistant fragments of phosphorylated TDP-43 are similarly different in accordance with the banding patterns seen in untreated C-terminal fragments, confirming the direct link between neuropathological subtypes and biochemical banding patterns. The mass spectrometric analysis indicated that the protease resistant regions

of abnormal TDP-43 are different between the diseases. As abnormally phosphorylated TDP-43 has been shown to accumulate in a filamentous form in ALS spinal cords (Hasegawa *et al.*, 2008), the filament core regions may be different between the diseases. Protease-resistant bands, and differences in banding patterns, have been reported in the prion diseases, Creutzfeldt–Jakob disease and bovine spongiform encephalopathy (Collinge *et al.*, 1996). Protease-resistant prion protein extracted from cases with new-variant Creutzfeldt–Jakob disease showed a different and characteristic pattern from that in cases with sporadic Creutzfeldt–Jakob disease, with the banding pattern being indistinguishable from that of mice infected with bovine spongiform encephalopathy prion. Protease-treated prion protein species are thought to have different mobilities because of different conformations. These observations in prion disease suggest that the different banding patterns to the abnormal TDP-43 fragments in ALS and FTLD might represent different TDP-43 strains with different conformations.

Recently, TDP-43 pathology has been detected in some cases with Alzheimer's disease (Arai *et al.*, 2009). We have shown here that the banding patterns of TDP-43 in cases of Alzheimer's disease with TDP-43 pathology are the same as those in FTLD-TDP type A. These novel observations suggest a biochemical commonality between FTLD and Alzheimer's disease with respect to TDP-43 pathology.

The results shown in this study also suggest a molecular basis for the clinicopathological classification of TDP-43 proteinopathies, which complements the histological classifications (Mackenzie *et al.*, 2011).

Funding

This work was supported by a Grant-in-Aid for Scientific Research (A) (to M.H., 11000624) from Ministry of Education, Culture, Sports, Science and Technology of Japan, and grants from Ministry of Health, Labor and Welfare of Japan (to M.H.).

Supplementary material

Supplementary material is available at *Brain* online.

References

Arai T, Mackenzie IR, Hasegawa M, Nonoka T, Niizato K, Tsuchiya K, et al. Phosphorylated TDP-43 in Alzheimer's disease and dementia with Lewy bodies. Acta Neuropathol (Berl) 2009; 117: 125–36.

Arai T, Hasegawa M, Akiyama H, Ikeda K, Nonaka T, Mori H, et al. TDP-43 is a component of ubiquitin-positive tau-negative inclusions in frontotemporal lobar degeneration and amyotrophic lateral sclerosis. Biochem Biophys Res Commun 2006; 351: 602–11.

Arai T, Ikeda K, Akiyama H, Nonaka T, Hasegawa M, Ishiguro K, et al. Identification of amino-terminally cleaved tau fragments that distinguish progressive supranuclear palsy from corticobasal degeneration. Ann Neurol 2004; 55: 72–9.

Armstrong RA, Ellis W, Hamilton RL, Mackenzie IR, Hedreen J, Gearing M, et al. Neuropathological heterogeneity in frontotemporal lobar degeneration with TDP-43 proteinopathy: a quantitative study of 94 cases using principal components analysis. J Neural Transm 2010; 117: 227–39.

Baker M, Mackenzie IR, Pickering-Brown SM, Gass J, Rademakers R, Lindholm C, et al. Mutations in progranulin cause tau-negative frontotemporal dementia linked to chromosome 17. Nature 2006; 442: 916–19.

Boeve BF, Boylan KB, Graff-Radford NR, Dejesus-Hernandez M, Knopman DS, Pedraza O, et al. Characterization of frontotemporal dementia and/or amyotrophic lateral sclerosis associated with the GGGGCC repeat expansion in *C9ORF72*. Brain 2012; 135: 765–83.

Braak H, Braak E. Neuropathological stageing of Alzheimer-related changes. Acta Neuropathol 1991; 82: 239–59.

Braak H, Del Tredici K, Rub U, de Vos RA, Jansen Steur EN, Braak E. Staging of brain pathology related to sporadic Parkinson's disease. Neurobiol Aging 2003; 24: 197–211.

Brooks BR. El Escorial World Federation of Neurology criteria for the diagnosis of amyotrophic lateral sclerosis. Subcommittee on Motor Neuron Diseases/Amyotrophic Lateral Sclerosis of the World Federation of Neurology Research Group on Neuromuscular Diseases and the El Escorial "Clinical limits of amyotrophic lateral sclerosis" workshop contributors. J Neurol Sci 1994; 124 (Suppl): 96–107.

Cairns NJ, Bigio EH, Mackenzie IR, Neumann M, Lee VM, Hatanpaa KJ, et al. Neuropathologic diagnostic and nosologic criteria for frontotemporal lobar degeneration: consensus of the Consortium for Frontotemporal Lobar Degeneration. Acta Neuropathol 2007a; 114: 5–22.

Cairns NJ, Neumann M, Bigio EH, Holm IE, Troost D, Hatanpaa KJ, et al. TDP-43 in familial and sporadic frontotemporal lobar degeneration with ubiquitin inclusions. Am J Pathol 2007b; 171: 227–40.

Clavaguera F, Bolmont T, Crowther RA, Abramowski D, Frank S, Probst A, et al. Transmission and spreading of tauopathy in transgenic mouse brain. Nat Cell Biol 2009; 11: 909–13.

Collinge J, Sidle KC, Meads J, Ironside J, Hill AF. Molecular analysis of prion strain variation and the aetiology of 'new variant' CJD. Nature 1996; 383: 685–90.

DeJesus-Hernandez M, Mackenzie IR, Boeve BF, Boxer AL, Baker M, Rutherford NJ, et al. Expanded GGGGCC hexanucleotide repeat in noncoding region of *C9ORF72* causes chromosome 9p-linked FTD and ALS. Neuron 2011; 72: 245–56.

Frost B, Jacks RL, Diamond MI. Propagation of tau misfolding from the outside to the inside of a cell. J Biol Chem 2009; 284: 12845–52.

Geser F, Brandmeir NJ, Kwong LK, Martinez-Lage M, Elman L, McCluskey L, et al. Evidence of multisystem disorder in whole-brain map of pathological TDP-43 in amyotrophic lateral sclerosis. Arch Neurol 2008; 65: 636–41.

Geser F, Martinez-Lage M, Robinson J, Uryu K, Neumann M, Brandmeir NJ, et al. Clinical and pathological continuum of multisystem TDP-43 proteinopathies. Arch Neurol 2009; 66: 180–9.

Gitcho MA, Bigio EH, Mishra M, Johnson N, Weintraub S, Mesulam M, et al. TARDBP 3'-UTR variant in autopsy-confirmed frontotemporal lobar degeneration with TDP-43 proteinopathy. Acta Neuropathol 2009; 118: 633–45.

Hasegawa M, Arai T, Nonaka T, Kametani F, Yoshida M, Hashizume Y, et al. Phosphorylated TDP-43 in frontotemporal lobar degeneration and amyotrophic lateral sclerosis. Ann Neurol 2008; 64: 60–70.

Hsiung GY, Dejesus-Hernandez M, Feldman HH, Sengdy P, Bouchard-Kerr P, Dwosh E, et al. Clinical and pathological features of familial frontotemporal dementia caused by *C9ORF72* mutation on chromosome 9p. Brain 2012; 135: 709–22.

Inukai Y, Nonaka T, Arai T, Yoshida M, Hashizume Y, Beach TG, et al. Abnormal phosphorylation of Ser409/410 of TDP-43 in FTLD-U and ALS. FEBS Lett 2008; 582: 2899–904.

Josephs KA, Ahmed Z, Katsuse O, Parisi JF, Boeve BF, Knopman DS, et al. Neuropathologic features of frontotemporal lobar degeneration with ubiquitin-positive inclusions with progranulin gene (*GRN*) mutations. J Neuropathol Exp Neurol 2007; 66: 142–51.

Kabashi E, Valdmanis PN, Dion P, Spiegelman D, McConkey BJ, Vande Velde C, et al. TARDBP mutations in individuals with sporadic and familial amyotrophic lateral sclerosis. Nat Genet 2008; 40: 572–4.